bioRxiv preprint doi: https://doi.org/10.1101/2023.10.17.562616; this version posted October 20, 2023. The copyright holder for this preprint (which was not certified by peer review) is the author/funder, who has granted bioRxiv a license to display the preprint in perpetuity. It is made available under aCC-BY-ND 4.0 International license.

Distinguishing mutants that resist drugs via different mechanisms by examining fitness tradeoffs across hundreds of fluconazole-resistant yeast strains

Kara Schmidlin[1,2*], Sam Apodaca[1,2*], Daphne Newell[1,2], Alexander Sastokas[1,2], Grant Kinsler[3], Kerry Geiler-Samerotte[1,2]

Abstract

There is growing interest in designing multidrug therapies that leverage tradeoffs to combat drug resistance. Tradeoffs are common in evolution and occur when, for example, resistance to one drug results in sensitivity to another. Major questions remain about the extent to which the mutants that provide resistance to a given drug all suffer similar tradeoffs. This question is difficult because the drug-resistant mutants observed in the clinic, and even those evolved in controlled laboratory settings, are often biased towards those that provide large fitness benefits. Thus, the mutations (and mechanisms) that provide drug resistance may be more diverse than current data suggests. Here, we perform evolution experiments utilizing lineage-tracking to capture a fuller spectrum of mutations that give yeast cells a fitness advantage in fluconazole, a common antifungal drug. We then quantify fitness tradeoffs for each of 774 evolved mutants across 12 environments, finding these mutants group into six classes with characteristically different tradeoffs. Their unique tradeoffs may imply that each group of mutants affects fitness through different molecular mechanisms. Some of the groupings we find are surprising. For example, we find some mutants that resist single drugs do not resist their combination, and some mutants to the same gene have different tradeoffs than others. These findings, on one hand, demonstrate the difficulty in relying on consistent or intuitive tradeoffs when designing multidrug treatments that thwart resistance. On the other hand, by demonstrating that hundreds of adaptive mutations can be reduced to a relatively smaller number of groups, our findings suggest that resistance evolves through a relatively small number of mechanisms, which may facilitate multidrug strategies to thwart resistance as well as more general evolutionary predictions. By grouping mutants that likely affect fitness through similar underlying mechanisms, our findings also inform efforts to map the phenotypic impacts of mutation.

Keywords: Fitness tradeoffs, drug resistance, DNA barcodes, fitness profiles, gene-by-environment interactions, molecular mechanisms, genotype-phenotype map, azole resistance

Introduction

How many different molecular mechanisms can a microbe exploit to adapt to a challenging environment? Answering this question is particularly urgent in the field of drug resistance because infectious populations are adapting to available drugs faster than new drugs are developed (Ventola 2015; Centers for Disease Control and Prevention (U.S.) 2019). Understanding the mechanistic basis of drug resistance can inform strategies for how to combine existing drugs in a way that prevents the evolution of resistance (Andersson and Hughes 2010; Melnikov et al. 2020; Pinheiro et al. 2021). For example, one strategy exposes an infectious population to one drug (Drug A) knowing that the mechanism of resistance to Drug A makes cells susceptible to Drug B (Hall et al. 2009; Pál et al. 2015; Baym et al. 2016; Roemhild et al. 2020). Problematically, these multi-drug strategies perform best when all mutants that resist Drug A have a tradeoff in the second drug (**Figure 1A**). If there are multiple different mechanisms to resist Drug A, some of which come with different tradeoffs, these treatment strategies could fail (**Figure 1B**), and they sometimes do (Grier et al. 2003; Abel zur Wiesch et al. 2014; Wang et al. 2019; Scarborough et al. 2020).

Laboratory experiments that have power to search for universal tradeoffs – where all the mutants that perform well in one environment perform poorly in another – often find there are mutants that violate trends or the absence of trends altogether (Hill et al. 2015; Nichol et al. 2019; Kinsler et al. 2020; Gjini and Wood 2021; Ardell and Kryazhimskiy 2021; Herren and Baym 2022). Another way to phrase this observation is to say that adaptive mutations often have effects in environments other than the one in which they originally evolved. These effects, referred to as 'pleiotropic' effects, are unpredictable and context dependent (Jerison et al. 2020; Geiler-Samerotte et al. 2020; Bakerlee et al. 2021; Chen et al. 2023). In sum, observations from many fields suggest that diverse mechanisms can improve a microbe's performance in a given environment resulting in diverse tradeoffs in other environments.

[1] Biodesign Center for Mechanisms of Evolution, Arizona State University, Tempe, AZ
[2] School of Life Sciences, Arizona State University, Tempe AZ
[3] University of Pennsylvania, Philadelphia, PA
Corresponding Author: kerry.samerotte@asu.edu

bioRxiv preprint doi: https://doi.org/10.1101/2023.10.17.562616; this version posted October 20, 2023. The copyright holder for this preprint (which was not certified by peer review) is the author/funder, who has granted bioRxiv a license to display the preprint in perpetuity. It is made available under aCC-BY-ND 4.0 International license.

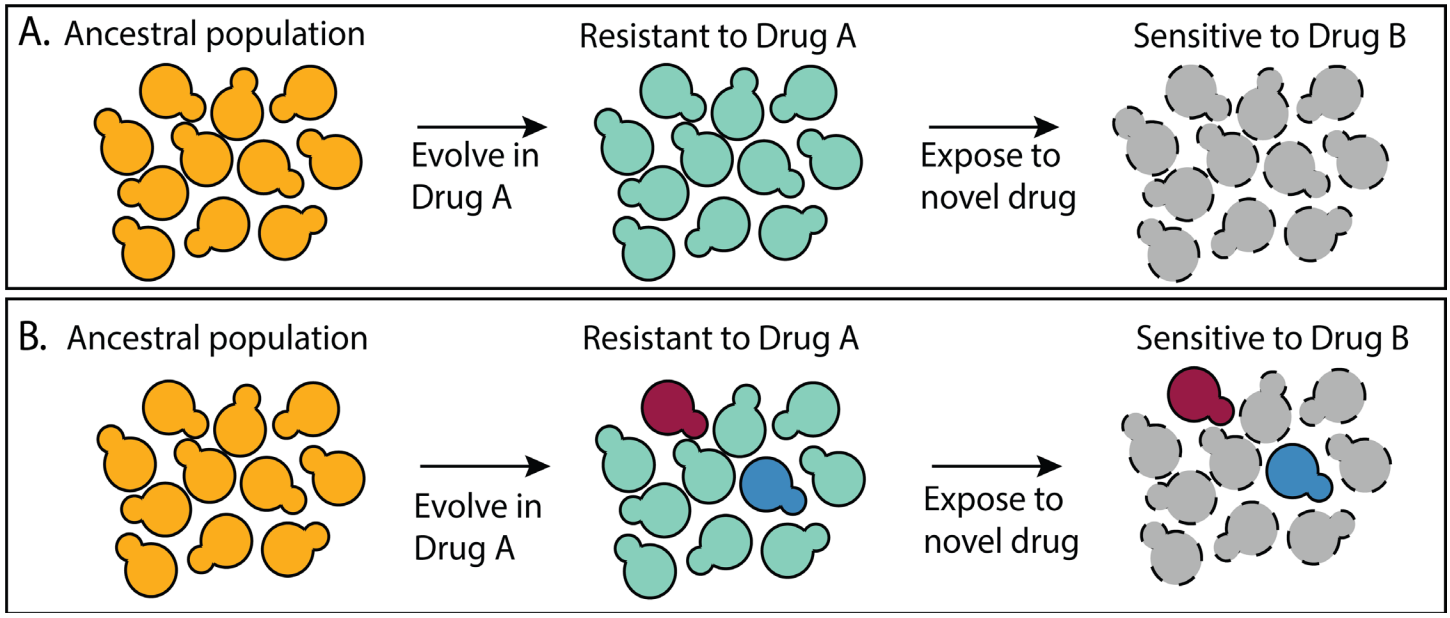

Figure 1: A multidrug treatment strategy that relies on all mutants having the same tradeoffs. (A) All of the mutants that resist Drug A do so via a similar mechanism such that all are sensitive to Drug B. **(B)** There are multiple different types of mutants that resist Drug A, not all of which are sensitive to Drug B.

A related conclusion is that our knowledge of the mechanisms contributing to adaptation, even adaptation resulting in resistance to widely used drugs, is incomplete. This gap in knowledge is partly due to the fact that mutations that provide the strongest fitness advantage often dominate evolution. Thus, in the clinic, and in laboratory experiments, the same drug-resistant mutations repeatedly emerge (Lupetti et al. 2002; Berkow and Lockhart 2017; Melnikov et al. 2020; Ksiezopolska et al. 2021), potentially leading to the false impression that the mechanistic basis of resistance to a particular drug is less varied than may be true. This problem is amplified by the limitations of most DNA sequencing methods, particularly that they cannot detect mutations present in less than 10% of cells (Good et al. 2017). The problem also reflects the expense of whole genome sequencing and the challenge of identifying novel adaptive mutations (Martínez and Lang 2023), both of which can encourage screens for known resistance mutations (Su et al. 2019) and impede searches for novel targets. In order to design better multi-drug treatment strategies that thwart resistance, or to see if such strategies are even feasible, we need methods to survey a more complete set of mutations (and mechanisms) that can contribute to adaptation.

Fortunately, single-cell and single-lineage DNA sequencing technologies are allowing us to more deeply sample genetic diversity in evolving populations of microbes (Schmidt and Efferth 2016). Here, we leverage a platform to perform massively-replicate evolution experiments in yeast. This platform has been shown to reveal the full spectrum of mutations underlying adaptation to a particular environment (Levy et al. 2015). The key to its success is that it uses DNA barcodes to track all competing adaptive lineages, not just the ones that ultimately rise to appreciable frequency. We apply this platform to investigate mechanisms underlying resistance to a specific antifungal drug: fluconazole (FLU) (Wang et al. 2022; Logan et al. 2022). Although serious fungal infections are most common in immunocompromised individuals, their impact on global health is still striking, resulting in over 1.5 million deaths annually (Xie et al. 2014; Iyer et al. 2022). Fungi are eukaryotes, which severely limits the number of possible drug targets that do not cause host toxicity (Xie et al. 2014). As a result, azoles are one of only three classes of antifungal drugs used to treat fungal infections. This amplifies the problem of drug resistance, as resistance to one azole commonly confers resistance to others of the same class, decreasing treatment options (Berman and Krysan 2020). By focusing on mechanisms of azole resistance, we to contribute to a growing literature about the tradeoffs that may be leveraged to design multidrug treatment strategies (Cowen and Lindquist 2005; Hill et al. 2015; Ksiezopolska et al. 2021; Iyer et al. 2022). However, our primary goal is more generic: we seek to explore the utility of a high-throughput evolutionary approach to enumerate the mechanisms of drug resistance.

To enhance the diversity of mechanisms underlying drug resistance in our experiment, we performed multiple laboratory evolutions in a range of FLU concentrations and sometimes in combination with a second drug. We did so because previous work has shown that different drug concentrations and combinations select for different azole resistance mechanisms (Cowen and Lindquist 2005; Hill et al. 2015). Ultimately, we obtained a large collection of 774 yeast strains that are adaptive in at least one of the environments we study from which we could begin to investigate the mechanistic basis of FLU-resistance.

But how do we go about deciphering the molecular mechanisms that contribute to drug resistance and susceptibility across such a large collection of mutants? Typical phenotyping methods, e.g., quantifying expression levels of drug export pumps (Miyazaki et al. 1998) or of the drug targets themselves (Palmer and Kishony 2014), are low throughput and require some a priori knowledge of the

bioRxiv preprint doi: https://doi.org/10.1101/2023.10.17.562616; this version posted October 20, 2023. The copyright holder for this preprint (which was not certified by peer review) is the author/funder, who has granted bioRxiv a license to display the preprint in perpetuity. It is made available under aCC-BY-ND 4.0 International license.

phenotypes that may be involved in resistance. Instead, many studies focus on identifying the genetic basis of adaptation in order to glean insights about the underlying mechanisms (Tenaillon et al. 2012; Cowen et al. 2014; Venkataram et al. 2016). However, genotyping lineages from barcoded pools is technically challenging (Venkataram et al. 2016), and further, genotype does not necessarily predict phenotype (Eguchi et al. 2019; Brettner et al. 2022b). For example, previous work using the same massively-replicate evolution platform that we use here discovered that many of mutations that provide an advantage in glucose-limited conditions are in genes comprising a canonical glucose-sensing pathway (Venkataram et al. 2016). Yet despite this similarity at the genetic level, follow-up work showed that these mutants did not all experience the same tradeoffs when exposed to new environments (Li et al. 2018b; Kinsler et al. 2020).

Instead of trying to identify the phenotypic or even the genetic basis of adaptation, here we strive to enumerate different classes of FLU-resistant mutants. Understanding how many different mutant classes exist informs questions about the feasibility (or infeasibility) of multi-drug therapy (**Figure 1**). We sort evolved FLU-resistant yeast strains into classes based on whether they share similar tradeoffs across environments. Previous work suggests that mutants with different fitness tradeoffs may affect fitness through different molecular mechanisms (Rodrigues et al. 2016; Li et al. 2019; Pinheiro et al. 2021). Our work is thus part of a growing push to flip the problem of mechanism on its head by, instead of using mechanism to predict fitness, using how fitness varies across environments to learn about the causative mechanisms underlying fitness differences (Li et al. 2019; Kinsler et al. 2020; Petti et al. 2023).

Across our collection of 774 adaptive yeast lineages we discovered at least six distinct groups with characteristic tradeoffs. For example, we find some drug resistant mutants are generally advantageous, while others are advantageous only in specific environments. And we find some mutants that resist single drugs also resist combinations of those drugs, while others do not. By grouping mutants with similar tradeoffs, we reduce the number of unique drug-resistant mutants from more than can be easily phenotyped (774) to a manageable panel for investigating the mechanistic basis of drug resistance.

With regard to drug regimens that exploit tradeoffs (**Figure 1**), our finding of multiple mutant classes with different tradeoffs suggests this may not be straightforward. The outlook is further complicated by our finding that some classes of FLU-resistant mutant primarily emerge from evolution experiments that did not contain FLU. This, as well as limits on our power to observe mutants with strong tradeoffs, suggest there may be additional mechanisms of FLU resistance beyond what we sampled (see (Cowen and Lindquist 2005)). Still, nuanced strategies to thwart resistance in cases where there are multiple types of resistant mutant are emerging (Maltas and Wood 2019; Gjini and Wood 2021; Wang et al. 2023). For example, one idea is to apply a drug regimen that enriches for mutants that suffer strong tradeoffs before exploiting those tradeoffs (Iram et al. 2020). Another idea is to perform single-cell sequencing on infectious populations to discover which classes of mutants are present (Nagasawa et al. 2021; Forsyth et al. 2021) and design treatments specific to those (Maltas and Wood 2019; Aissa et al. 2021; Hsieh et al. 2022). Our findings support that such ideas may be feasible by demonstrating that there are not as many unique fitness tradeoffs as there are mutations. Our work – showing that 774 mutants fall into a much smaller number of groups – contributes to growing literature suggesting that the phenotypic basis of adaptation is not as diverse as the genetic basis (Kinsler et al. 2020; Iwasawa et al. 2022; Petti et al. 2023). This winnowing of diversity may make evolutionary processes, for example, whether an infectious population will adapt to resist a drug, somewhat more predictable (Rodrigues et al. 2016; Lässig et al. 2017; Kinsler et al. 2020; Yoon et al. 2021; King et al. 2022; Wortel et al. 2023).

Results

Barcoded evolution experiments uncover hundreds of yeast lineages with adaptive mutations

In order to create a sizable collection of drug-resistant mutants, we performed high-replicate evolution experiments utilizing barcoded yeast (Levy et al. 2015; Li et al. 2018b; Boyer et al. 2021). This barcoding system allows evolving hundreds of thousands of genetically identical yeast lineages together in a single flask. Each lineage is tagged with a unique DNA barcode, which is a 26 base pair sequence of DNA located within an artificial intron. Lineages with unique barcodes can be thought of as independent replicates of an evolution experiment. This high-replicate system has the potential to generate many different yeast lineages that differ by single adaptive mutations (Venkataram et al. 2016; Kinsler et al. 2020).

We performed a total of 12 barcoded evolution experiments, each of which started from the same pool of approximately 300,000 barcoded yeast lineages (**Figure S1**). These evolutions survey how yeast cells adapt to different concentrations and combinations of two drugs: fluconazole (FLU) and radicicol (RAD) (**Table 1**). FLU is a first line of defense against yeast infections, but over the past two decades diverse resistant mutations have been identified (Bongomin et al. 2017; Rybak et al. 2022; Osset-Trénor et al. 2023). Some earlier work suggested that FLU-resistant mutants are sensitive to the second drug we study, radicicol (RAD) (Cowen and Lindquist 2005; Cowen et al. 2009), and more generally that RAD can prevent the emergence of drug resistance in other systems (Whitesell et al. 2014). However, there are some mutants that are cross resistant to both FLU and RAD (Hill et al. 2015), and the prominent mechanism of resistance can differ with the intensity of selection and drug concentration (Cowen and Lindquist 2005; Yang et al. 2023). We thus chose to evolve yeast to resist different concentrations and combinations of FLU and RAD to generate a diverse pool of adaptive mutations comprising different mechanisms of drug resistance.

We evolved yeast to resist three different concentrations of either FLU and RAD for a total of six single-drug conditions

bioRxiv preprint doi: https://doi.org/10.1101/2023.10.17.562616; this version posted October 20, 2023. The copyright holder for this preprint (which was not certified by peer review) is the author/funder, who has granted bioRxiv a license to display the preprint in perpetuity. It is made available under aCC-BY-ND 4.0 International license.

Evolution Condition	Abbreviation	SYMBOL
4 µg/ml Fluconazole	Low Flu	
6 µg/ml Fluconazole	Med Flu	
8 µg/ml Fluconazole	High Flu	
5 µM Radicicol	Low Rad	
15 µM Radicicol	Med Rad	
20 µM Radicicol	High Rad	
5 µM Radicicol + 4 µg/ml Fluconazole	LRLF	
5 µM Radicicol + 8 µg/ml Fluconazole	LRHF	
15 µM Radicicol + 4 µg/ml Fluconazole	HRLF	
15 µM Radicicol +8 µg/ml Fluconazole	HRHF	
0.5% DMSO	DMSO	
No Drug	No Drug	

Table 1: A list of the environments included in this study

(**Table 1**). We also studied four conditions containing combinations of both drugs, as well as two control conditions, for a total of 12 evolution experiments (**Table 1**). We chose to study subclinical drug concentrations with the hope that no drug treatment would be strong enough to reduce the population of yeast cells to only a handful of unique barcodes (**Figure S2**). We needed to maintain barcode diversity in order to evolve a large number of unique lineages that each accumulate different mutations.

With the goal of collecting adaptive lineages from each evolution experiment, we took samples from each of our 12 barcoded evolutions after 3 - 6 growth/transfer cycles (**Figure S1**). This represents roughly 24 to 48 generations of growth assuming 8 generations per growth/transfer cycle (Levy et al. 2015). We sampled early because previous work using this barcoded evolution system demonstrated that the diversity of adaptive lineages is highest after just a few dozen generations (Levy et al. 2015; Venkataram et al. 2016). We sampled about 2,000 cells from each evolution experiment except those three containing high FLU from which we sampled only 1,000 cells. We then tested our sampled lineages for the presence of adaptive mutations by measuring the fitness of all ~21,000 isolates (2,000 cells x 9 conditions + 1000 cells x 3 conditions) relative to their ancestor (Venkataram et al. 2016). To do so, we pooled these 21,000 isolates and used this pool to initiate fitness competition experiments. We competed the pool against control strains, i.e., strains of the ancestral genotype that do not possess adaptive mutations (Venkataram et al. 2016; Kinsler et al. 2020). We performed 24 such competitive fitness experiments, 2 per each of the original 12 evolution conditions. In each experiment, we emulated the growth and transfer conditions of the original evolution experiments as precisely as possible, tracking how barcode frequencies changed over 5 growth/transfer cycles (~40 generations). We used the log-linear slope of this change, relative to the average slope for the control strains, to quantify relative fitness.

We found many barcodes had slopes that were more positive than the control strains, suggesting that they possess adaptive mutations that improved their fitness (**Figure S3**). In fact, some of these adaptive lineages outcompeted the other lineages so quickly that it posed a challenge. Barcodes pertaining to outcompeted lineages were often not present at high enough coverage to track their fitness. We applied a conservative filter, preserving only 774 lineages with barcodes that were observed >500 times in at least one replicate experiment per each of the 12 environments. Lineages that have low fitness rarely pass this filter, thus our 774 lineages are biased towards those that are reproducibly adaptive in the environments we study (**Figure S4**). Despite this biased sample, we will go on to demonstrate that there are likely many different mechanisms of adaptation represented among these 774 lineages.

To provide evidence that these 774 barcoded yeast lineages indeed possess adaptive mutations, we performed whole genome sequencing on a subset of 62 strains. Because we sampled these lineages after only a few dozen generations of evolution, each lineage differs from the ancestor by just a few mutations, making it easy to pinpoint the genetic basis of adaptation. Doing so revealed mutations that have previously been shown to be adaptive in our evolution conditions (**Table S1**). For example, we sequenced many FLU-resistant yeast lineages finding 35 with unique single nucleotide mutations in either PDR1 or PDR3, and a few with mutations in SUR1 or UPC2, genes which have all been shown to contribute to FLU resistance in previous work (Flowers et al. 2012; Vasicek et al. 2014; Tanaka and Tani 2018; Uemura and Moriguchi 2022; Vu and Moye-Rowley 2022). Similarly, lineages that have very high fitness in RAD were found to possess single nucleotide mutations in genes associated with RAD resistance, such as HDA1 (Robbins et al. 2012) and HSC82, which is the target of RAD (Roe et al. 1999). We also observed several lineages with similar mutations to those observed in other studies using this barcoded evolution regime, including mutations to IRA1, IRA2 and GPB2 (Venkataram et al. 2016; Kinsler et al. 2020). Previous barcoded evolutions also observed that increases in ploidy were adaptive, with 43 to 60% of cells becoming diploid during the course of evolution (Venkataram et al. 2016). However, ploidy changes contributed less to adaptation in our experiment, with at most 9.4% of cells becoming diploid by the time point when we sampled, but often less than 2% (**Table S2**). In sum, we conclude that we have created a diverse pool of 774 barcoded yeast lineages, most of which have a fitness advantage in one of the conditions we study and are likely to possess a unique adaptive mutation. The question we address for the rest of this study is to what extent these hundreds of mutant lineages differ from one another in terms of the mechanism/s underlying their fitness advantages.

bioRxiv preprint doi: https://doi.org/10.1101/2023.10.17.562616; this version posted October 20, 2023. The copyright holder for this preprint (which was not certified by peer review) is the author/funder, who has granted bioRxiv a license to display the preprint in perpetuity. It is made available under aCC-BY-ND 4.0 International license.

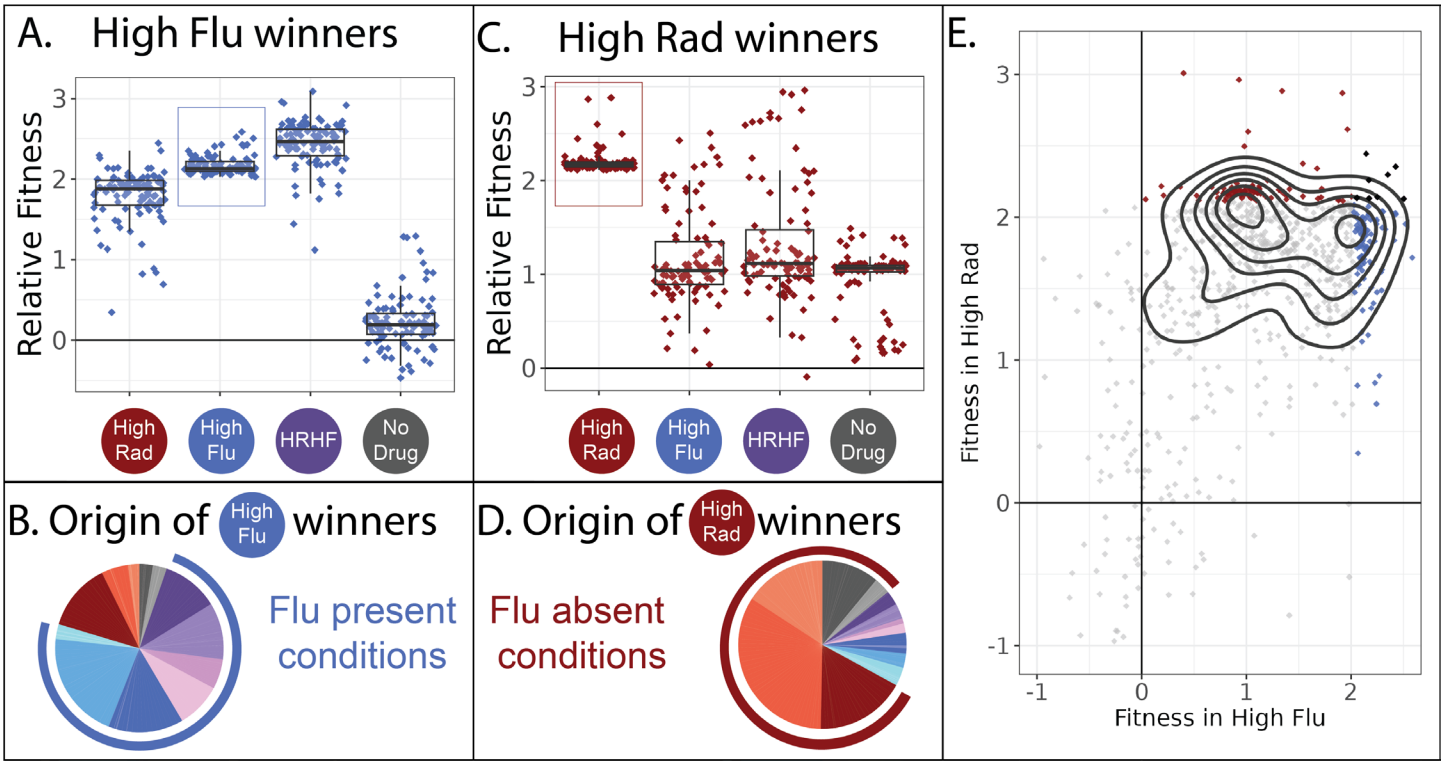

Figure 2: Two different classes of FLU-resistant mutants with unique tradeoffs. (**A**) This panel describes the 100 mutant lineages with the highest fitness relative to the control strains in the high FLU environment (8µg/ml FLU). The vertical axis depicts the fitnesses (log-linear slopes relative to control strains) for these 100 strains in four selected environments, including the high FLU environment (boxed). Boxplots summarize the distribution across all 100 lineages for each environment, displaying the median (center line), interquartile range (IQR) (upper and lower hinges), and highest value within 1.5 × IQR (whiskers). (**B**) The 100 lineages with highest fitness in high FLU were most often sampled from evolution experiments containing FLU. (**C**) Similar to panel A, this panel describes the 100 mutant lineages with the highest fitness relative to the control strains in the high RAD environment (20uM Rad). (**D**) The 100 lineages with highest fitness in high RAD were most often sampled from evolution experiments that did not contain FLU, and yet they provide a fitness advantage in the high FLU condition. (**E**) A pairwise correlation plot showing that all 774 mutants, not just the two groups of 100 depicted in panels A and C, to some extent fall into two groups defined by their fitness in high FLU and high RAD. The contours (black curves) were generated using kernel density estimation with bins = 7. These contours describe the density of the underlying data, which is concentrated into two clusters defined by the two smallest black circles. The 100 mutants with highest fitness in high FLU are blue, highest fitness in high RAD are red, and the seven that overlap between the two aforementioned categories are black.

A unique mechanisms of FLU resistance emerges among mutants isolated in RAD evolutions

The majority of the 774 adaptive lineages that we study have higher fitness than the ancestral strains in not one, but often in several drug conditions. This suggests that pleiotropy, and in particular cross-resistance, is prevalent among the lineages we study. But not all lineages show the same patterns of cross resistance (**Figure 2**). For example, the 100 most fit lineages in our highest concentration of fluconazole are also beneficial in our highest concentration of radicicol (**Figure 2A; leftmost two boxplots**). As expected, these 100 lineages also have high fitness in conditions where high concentrations of FLU and RAD are combined (**Figure 2A; third boxplot**). And these 100 most-fit lineages in FLU lose their fitness advantage in conditions where no drug is present (**Figure 2A; rightmost boxplot**).

Given their high fitness in conditions containing FLU, it seems likely that these 100 mutants originated from evolution experiments containing FLU. Before we pooled the lineages we sampled from each of our 12 evolution experiments, we independently sequenced each sample. This allows us to trace every lineage back to the evolution experiment/s it originated from. As we expected, these 100 best performing lineages in high FLU largely originate from evolution experiments containing FLU (**Figure 2B**). Given that these lineages have no fitness advantage in conditions containing no drug, it is also unsurprising that they are underrepresented in evolution experiments lacking RAD and FLU (**Figure 2B**).

It might be tempting to generalize that most mutations that provide drug resistance are not beneficial in environments without drugs. Afterall, we show this is true for a large number of independent lineages (**Figure 2A**). Further, many previous studies find a similar pattern, whereby drug resistant mutants often do not have high fitness in the absence of drug (Andersson and Hughes 2010; Basra et al. 2018; Allen et al. 2019; Melnikov et al. 2020), such that treatment strategies have emerged that cycle patients between drug and no drug states, albeit with mixed success (Baker et al. 2018; Raymond 2019; Wang et al. 2019; Algazi et al. 2020). However, this type of generalization is not supported by our data. We find that drug resistance can sometimes come with an advantage, rather than a cost, in the absence of a drug (**Figure 2C**). The top 100 most fit mutants in our highest concentration of RAD provide a fitness advantage in high RAD, high FLU, as well as in environments with no drug (**Figure 2C**). These observations suggest that there are at least two different mechanisms by which to resist FLU that result in different tradeoffs in other environments (**Figure 2A vs. 2C**).

bioRxiv preprint doi: https://doi.org/10.1101/2023.10.17.562616; this version posted October 20, 2023. The copyright holder for this preprint (which was not certified by peer review) is the author/funder, who has granted bioRxiv a license to display the preprint in perpetuity. It is made available under aCC-BY-ND 4.0 International license.

Intriguingly, these multidrug resistant lineages that maintain their fitness advantage in the absence of drug (**Figure 2C**) mainly originate from evolution experiments performed in conditions lacking FLU (**Figure 2D**). This highlights how the potential mechanisms by which a microbe can resist a drug may be more varied than is often believed. Typically, one doesn't search for FLU-resistant mutants by evolving yeast to resist RAD. Thus typical studies might miss this unique class of FLU-resistant mutants.

In sum, there appear to be at least two different types of mutants present among our collection of 774 adaptive yeast lineages. One group has almost equally high fitness in RAD and FLU but has no fitness advantage over the ancestral strain in conditions without either drug (**Figure 2A & 2E**). Another group is defined by very high fitness in RAD, moderately high fitness in FLU and moderately high fitness in conditions without either drug (**Figure 2C & 2E**). When comparing fitness in RAD vs. FLU across all 774 lineages, not only the top 100 best performing in each drug, we see some evidence that they largely fall into the two main categories highlighted in **figures 2A and 2C** (**Figure 2E**). Thus it might be tempting to conclude that there are two different types of FLU-resistant mutant in our dataset. However, sorting mutants into groups using a pairwise correlation plot (**Figure 2E**) excludes data from ten of our twelve environments.

A strategy to differentiate classes of drug-resistant mutants with different tradeoffs

The observation of two distinct types of adaptive mutants (**Figure 2**) made us wonder whether there were additional unique types of FLU-resistant mutants with their own characteristic tradeoffs. This is difficult to tell by using pairwise correlation like that in **Figure 2E** because we are not studying pairs of conditions, as is somewhat common when looking for tradeoffs to leverage in multidrug therapies (Scarborough et al. 2020; Melnikov et al. 2020; Ardell and Kryazhimskiy 2021; Larkins-Ford et al. 2022). Instead, we have collected fitness data from across 12 conditions to yield a more comprehensive set of gene-by-environment interactions for each mutant. This type of data, describing how a particular genotype responds to environmental change, is sometimes called a 'reaction norm' and can inform quantitative genetic models of how selection operates in fluctuating environments (Gomulkiewicz and Kirkpatrick 1992; Ogbunugafor 2022) and how much pleiotropy exists in nature (Yadav et al. 2015). More recent studies refer to the changing performance of a genotype across environments as a 'fitness profile' or in aggregate, a 'fitness seascape,' and suggest these type of dynamic measurements are the key to designing effective multi-drug treatments (King et al. 2022) and to predicting evolution (Lässig et al. 2017; Kinsler et al. 2020; Cairns et al. 2022; Iwasawa et al. 2022; Chen et al. 2023). And when the environments studied represent different drugs, these types of data are often referred to as "collateral sensitivity profiles" a term chosen to convey how resistance to one drug can have "collateral" effects on performance in other drugs (Pál et al. 2015; Maltas and Wood 2019; Gjini and Wood 2021). Despite the wide interest in this type of fitness data, it is technically challenging to generate, thus many previous studies of fitness profiles focus on a much smaller number of isolates (Imamovic et al. 2018; Nichol et al. 2019; Maltas and Wood 2019), sometimes with variation restricted to a single gene (Mira et al. 2015; King et al. 2022), or evolved in response to a single selection pressure (Li et al. 2018b; Kinsler et al. 2020). Here, we have generated fitness profiles for a large and diverse group of drug-resistant strains using the power of DNA barcodes. Now we seek to understand whether these mutants fall into distinct classes that each have characteristic fitness profiles (i.e., characteristic tradeoffs, characteristic reaction norms, or characteristic gene-by-environment interactions).

To address this question, we perform dimensional reduction, clustering mutants with fitness profiles that have a similar shape. It is in theory possible for all mutants to have similar profiles, perhaps implying they all affect fitness through similar underlying mechanisms (**Figure 3A**). However, the disparity reported in **Figure 2** suggests otherwise. It's also possible that every mutant will have a different profile. This could happen if each mutant affects different molecular-level phenotypes that underlie its drug resistance (**Figure 3B**). But previous work suggests that the phenotypic basis of adaptation is less diverse than the genotypic basis. This is important because it means that evolutionary outcomes are more predictable at the level of phenotype (Kinsler et al. 2020; Brettner et al. 2022b; Iwasawa et al. 2022). Even so, every mutant could have a slightly different fitness profile if each affects the same handful of molecular-level phenotypes but to relatively different degrees. This would allow every mutant to have a unique response to environmental change, without requiring that there be as many unique molecular mechanisms underlying drug resistance as there are mutants. A final possibility is that there exist discrete classes of drug-resistant mutants with characteristic tradeoffs (**Figure 3C**). This might imply that each class of mutants provides drug resistance via a different molecular mechanism, or a different set of mechanisms. In sum, our endeavor to enumerate mutants with different fitness profiles speaks to general questions about the extent of pleiotropy in the genotype-phenotype-fitness map (Boyle et al. 2017; Geiler-Samerotte et al. 2020; Bakerlee et al. 2021; Chen et al. 2023), the extent to which fitness tradeoffs are universal (Andersson and Hughes 2010; Li et al. 2019; Herren and Baym 2022), and relatedly, the predictability of evolution and potential for controlling evolutionary processes (Lässig et al. 2017; Iram et al. 2020; Kinsler et al. 2020; King et al. 2022; Petti et al. 2023).

To see whether there are distinct classes of adaptive mutants among our drug-resistant yeast lineages, we applied uniform manifold approximation and projection (UMAP) (McInnes et al. 2018a) to fitness measurements for 774 yeast strains across all 12 environments. This method places mutants with similar fitness profiles near each other in two-dimensional space. As might be expected, it largely places mutants in each of the two categories described in **Figure 2** far apart, with drug-resistant mutants that lose their benefit in the absence of drug in the top half of the graph, and those that maintain their benefit in the bottom half (**Figure 3D** & **Figure**

bioRxiv preprint doi: https://doi.org/10.1101/2023.10.17.562616; this version posted October 20, 2023. The copyright holder for this preprint (which was not certified by peer review) is the author/funder, who has granted bioRxiv a license to display the preprint in perpetuity. It is made available under aCC-BY-ND 4.0 International license.

S5).

Beyond the obvious divide between the top and bottom clusters of mutants on the UMAP, we used a gaussian mixture model (Fraley and Raftery 2003) to identify clusters. A common problem in this type of analysis is the risk of dividing the data into clusters based on variation that represents measurement noise rather than reproducible differences between mutants (Zhao et al. 2008; Mirkin 2011). One way we avoided this was by ceasing to split out additional clusters before doing so no longer improved model performance (**Figure S6**). The model we chose consists of seven clusters, including one pertaining to the control strains, and six others pertaining to different classes of adaptive mutant (**Figure 3D**). We investigated whether these clusters capture reproducible differences between mutants, rather than measurement noise, by reducing the amount of noise in our data and asking if the same clusters are still present. To do so, we reduced our collection of adaptive lineages from 774

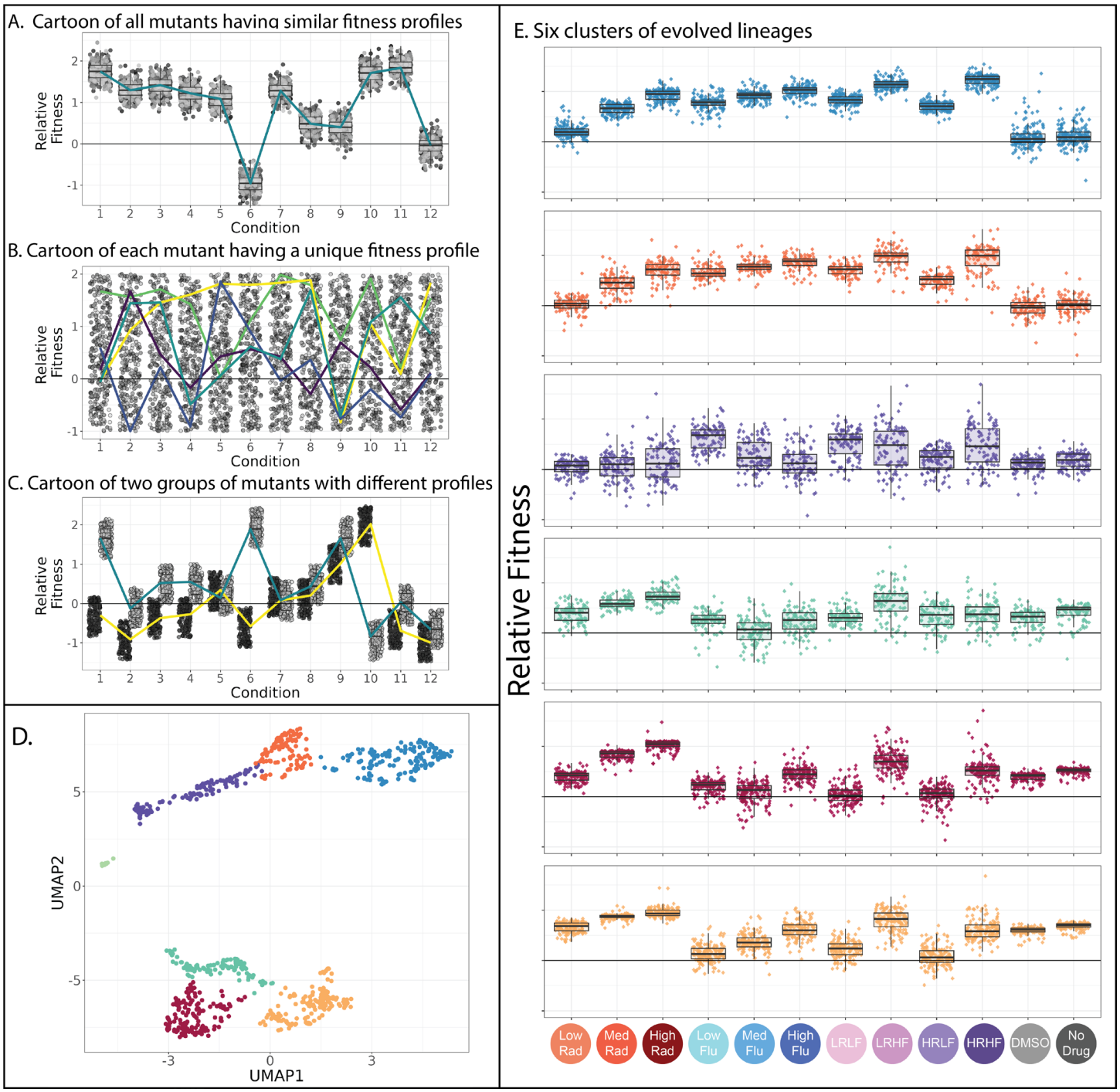

Figure 3: Clustering evolved lineages with similar fitness profiles. (**A-C**) Simulated data showing potential fitness profiles when (**A**) all mutants have similar responses to environmental change and thus a similar fitness profile, (**B**) every mutant has a different profile (five unique profiles are highlighted in color), or (**C**) every mutant has one of a small number of unique profiles (two unique profiles are depicted). (**D**) Every point in this plot represents one of the barcoded lineages colored by cluster; clusters were identified using a gaussian mixture model. The 774 adaptive lineages cluster into 6 groups based on variation in their fitness profiles; the control lineages cluster separately into the leftmost cluster in light green. (**E**) The fitness profiles of each cluster of adaptive lineages. Boxplots summarize the distribution across all lineages within each cluster in each environment, displaying the median (center line), interquartile range (IQR) (upper and lower hinges), and highest value within 1.5 × IQR (whiskers).

bioRxiv preprint doi: https://doi.org/10.1101/2023.10.17.562616; this version posted October 20, 2023. The copyright holder for this preprint (which was not certified by peer review) is the author/funder, who has granted bioRxiv a license to display the preprint in perpetuity. It is made available under aCC-BY-ND 4.0 International license.

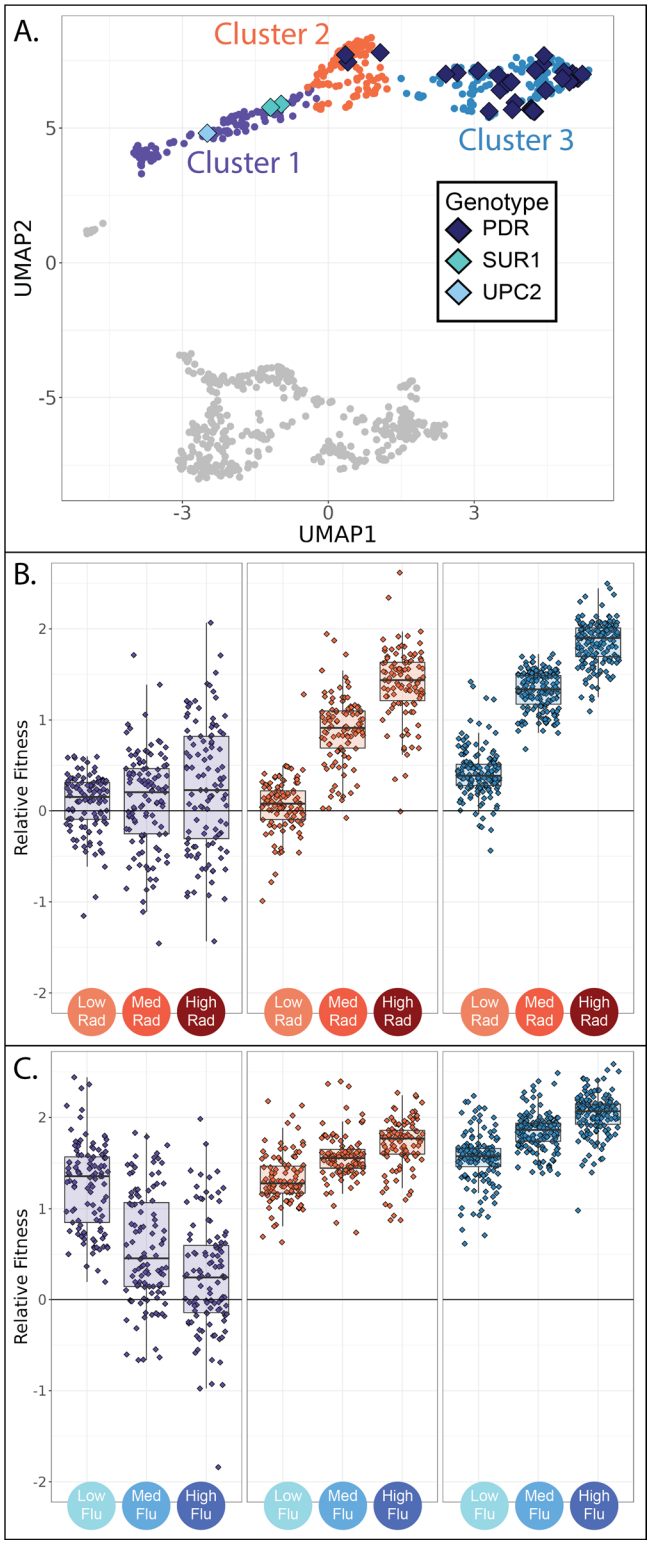

Figure 4: Evolved lineages comprising cluster 1 have different genotypes and phenotypes from neighboring clusters. (**A**) The three clusters on the top half of the UMAP differ in their targets of adaptation with cluster 1 being unique in that it does not contain mutations to PDR1 or PDR3. (**B**) Evolved lineages comprising cluster 1 do not have consistent fitness advantages in conditions containing RAD, while lineages comprising clusters 2 and 3 are uniformly adaptive in RAD. Boxplots summarize the distribution across all lineages within each cluster in each environment, displaying the median (center line), interquartile range (IQR) (upper and lower hinges), and highest value within 1.5 × IQR (whiskers). (**C**) Lineages comprising cluster 1 are most fit in low concentrations of FLU, and this advantage dwindles as the FLU concentration increases. Lineages comprising clusters 2 and 3 show the opposite trend.

to 617 by requiring 5,000 rather than 500 reads per lineage in order to infer fitness. This procedure reduced noise; the Pearson correlation across replicate experiments improved from 0.756% to 0.813%. Despite this reduction in variation, these 617 lineages cluster into the same six groups (plus a seventh pertaining to the control strains) as do the original 774 (**Figure S7**). The groupings are also preserved when we perform alternate methods for dimensionality reduction while adhering to a seven cluster model (**Figure S8**). Each of the six clusters of adaptive mutants that we identify has a characteristic fitness profile (**Figure 3E**). In any given environment, the fitnesses of the mutants within each cluster are often very similar to one another and often significantly different from other clusters (**Figure 3E**). Our follow-up investigations provide additional evidence that these clusters of adaptive mutants each have characteristically different tradeoffs, suggesting they affect fitness via different molecular mechanisms.

A group of mutants with distinct genotypes are primarily resistant to low concentrations of FLU

The upper three clusters of mutants on the UMAP (**Figure 3D**) are all similar in that they have elevated fitness in at least one FLU-containing environment but ancestor-like fitness in the absence of drug (**Figure 3E; upper three profiles**). Despite these similarities, there are major differences between these three groups of mutant lineages, both at the level of genotype and fitness profile (**Figure 4**). For example, in cluster 1 (depicted in purple in **Figures 3** & **4**), the 3 sequenced lineages have single nucleotide mutations to either SUR1 or UPC2 (**Figure 4A**). But in clusters 2 and 3 (depicted in blue and orange in **Figures 3** & **4**), 35/36 sequenced lineages have unique single nucleotide mutations to one of two genes associated with 'Pleiotropic Drug Resistance' (PDR1 or PDR3).

PDR1 and PDR3 are transcription factors that are well known to contribute to fluconazole resistance through increased transcription of a drug pump (PDR5) that removes FLU from cells (Fardeau et al. 2007; Osset-Trénor et al. 2023). However, SUR1 and UPC2 are less commonly mentioned in literature pertaining to FLU resistance, and have different functions within the cell as compared to PDR1 and PDR3 (Kapitzky et al. 2010; Hill et al. 2015). SUR1 converts inositol phosphorylceramide to mannosylinositol phosphorylceramide, which is a component of the plasma membrane (Uemura and Moriguchi 2022). Similarly, UPC2 is a transcription factor with a key role in activating the ergosterol biosynthesis genes, which contribute to membrane formation (Vik and Rine 2001; Tan et al. 2022). The presence of adaptive mutations in genes involved in membrane synthesis is consistent with fluconazole's disruptive effect on membranes (Sorgo et al. 2011).

Interestingly, the lineages with mutations to UPC2 and SUR1, and the unsequenced lineages in the same cluster, do not consistently have cross resistance in RAD (**Figure 4B; cluster 1**). Oppositely, lineages with mutations to PDR1 or PDR3, and the unsequenced lineages in the same clusters, are uniformly cross resistant to RAD (**Figure 4B; clusters 2**

bioRxiv preprint doi: https://doi.org/10.1101/2023.10.17.562616; this version posted October 20, 2023. The copyright holder for this preprint (which was not certified by peer review) is the author/funder, who has granted bioRxiv a license to display the preprint in perpetuity. It is made available under aCC-BY-ND 4.0 International license.

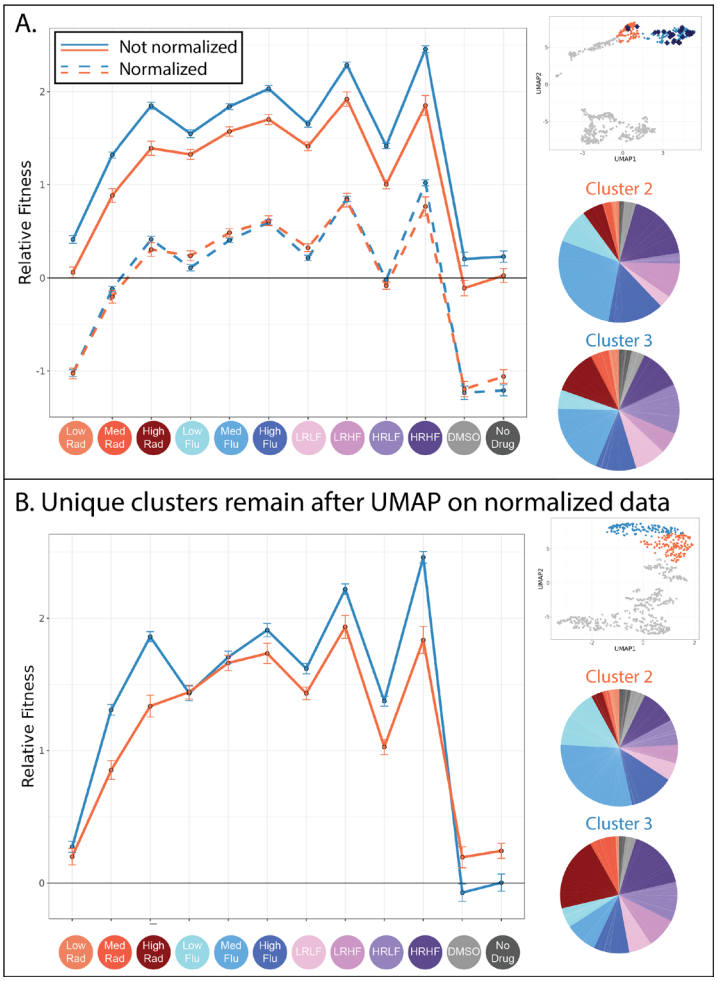

Figure 5: Evolved lineages in clusters 2 and 3 have characteristic differences despite similarities at the genetic level. (**A**) This panel shows the similarities between clusters 2 and 3. The upper right inset displays the same UMAP from **Figure 3D** with only clusters 2 and 3 highlighted and with lineages possessing mutations to the PDR genes depicted as blue diamonds. The line plot displays the same fitness profiles for clusters 2 and 3 as **Figure 3E**, plotting the average fitness for each cluster in each environment and a 95% confidence interval. Dotted lines represent the same data, normalized such that every lineage has an average fitness of 0 across all environments. These line plots show that the fitness profiles for clusters 2 and 3 have a very similar shape. Pie charts display the relative frequency with which lineages in clusters 2 and 3 were sampled from each of the 12 evolution conditions, colors match those in the horizontal axis of the line plot and table 1. (**B**) This panel shows the differences between the new clusters 2 and 3 created after fitness profiles were normalized to eliminate magnitude differences. The upper right inset displays a new UMAP (also see **Figure S9**) that summarizes from variation in fitness profiles after each profile was normalized by setting its average fitness to 0. The line plot displays the fitness profiles for the new clusters 2 and 3, which look different from those in panel A because 37% of mutants in the original clusters 2 and 3 switched identity from 2 to 3 or vice versa. The new clusters 2 and 3 are depicted in slightly different shades of blue and orange to reflect that these are not the same groupings as those depicted in **Figure 3**. Pie charts display the relative frequency with which lineages in new clusters 2 and 3 were sampled from each of the 12 evolution conditions, colors match those in the horizontal axis of the line plot and **table 1**.

and 3). Perhaps this cross resistance is reflective of the fact that the drug efflux pump that PDR1/3 regulates (PDR5) can transport a wide range of drugs and molecules out of yeast cells (Kolaczkowski et al. 1996; Harris et al. 2021). Overall, the targets of adaptation in cluster 1 have disparate functions within the cell as compared to the targets of adaptation in clusters 2 and 3. This may suggest that the mutants in cluster 1 confer FLU resistance via a different mechanism than clusters 2 and 3.

The lineages in cluster 1 have additional important differences from clusters 2 and 3. The lineages in cluster 1 perform best in the lowest concentration of FLU and have decreasing gains as the concentration of FLU rises (**Figure 4C**). In fact, about 15% of these mutant lineages perform worse than their ancestor in the highest concentration of FLU, suggesting the very mutations that provide resistance to low FLU are costly in higher concentrations of the same drug. The mutants in clusters 2 and 3 show the opposite trend from those in cluster 1: they perform best in the highest concentration of FLU and have reduced gains in lower concentrations (**Figure 4C**). These findings provide additional evidence that a distinct mechanism of FLU resistance distinguishes cluster 1 from clusters 2 and 3. The implication that different resistance mechanisms will dominate evolution in slightly different concentrations of the same drug highlights the complexity of adaptation and the need to more deeply understand the diversity of potential adaptive mechanisms before designing treatment strategies (Berman and Krysan 2020; Yang et al. 2023).

Two groups of mutant lineages possessing similar adaptive mutations differ in sensitivity to RAD

While cluster 1 appears fairly different from its neighbors, it is not immediately obvious why the mutant lineages in clusters 2 and 3 are placed into separate groups. For one, the mutants in each cluster have fitness profiles with a very similar shape (**Figure 3E & 5A**). The sequenced lineages in each of these clusters also possess mutations to the same genes: PDR1 and PDR3 (**Figure 4A**). And finally, the lineages in each cluster originate from similar evolution experiments, largely those containing FLU (**Figure 5B**; pie charts). These observations made us wonder whether the difference between cluster 2 and 3 arose entirely because the mutants in cluster 3 have stronger effects than those in cluster 2 (**Figure 5A**; the solid blue line is above the solid orange line). In other words, we wondered whether the mutant lineages in clusters 2 and 3 affect fitness via the same mechanism, but to different degrees. To investigate this idea, we normalized all fitness profiles to have the same height on the vertical axis; this does not affect their shape (**Figure 5A**; dotted lines). Then we re-clustered and asked whether mutants pertaining to the original clusters 2 and 3 were now merged into a single cluster.

Normalizing in this way did not radically alter the UMAP, which still contains largely the same 6 clusters of mutants (**Figure S9**). Clusters 2 and 3, containing lineages with mutations to PDR1 or PDR 3, experienced the largest changes with 37% of mutants switching from one of these two groups to the other. The new clusters 2 and 3 now differ in the shape of their fitness profiles, whereby slight differences that existed between the original fitness profiles are exaggerated (**Figure 5B**). For example, mutants in cluster 3 perform better in high and medium concentrations of RAD (**Figure 5B**). This difference in fitness is reflected in the evolution experiments, with more mutant lineages in cluster 3 originating from the evolutions performed in RAD (**Figure 5B**). Though cluster 3 mutants tend to have stronger RAD resistance, they tend

bioRxiv preprint doi: https://doi.org/10.1101/2023.10.17.562616; this version posted October 20, 2023. The copyright holder for this preprint (which was not certified by peer review) is the author/funder, who has granted bioRxiv a license to display the preprint in perpetuity. It is made available under aCC-BY-ND 4.0 International license.

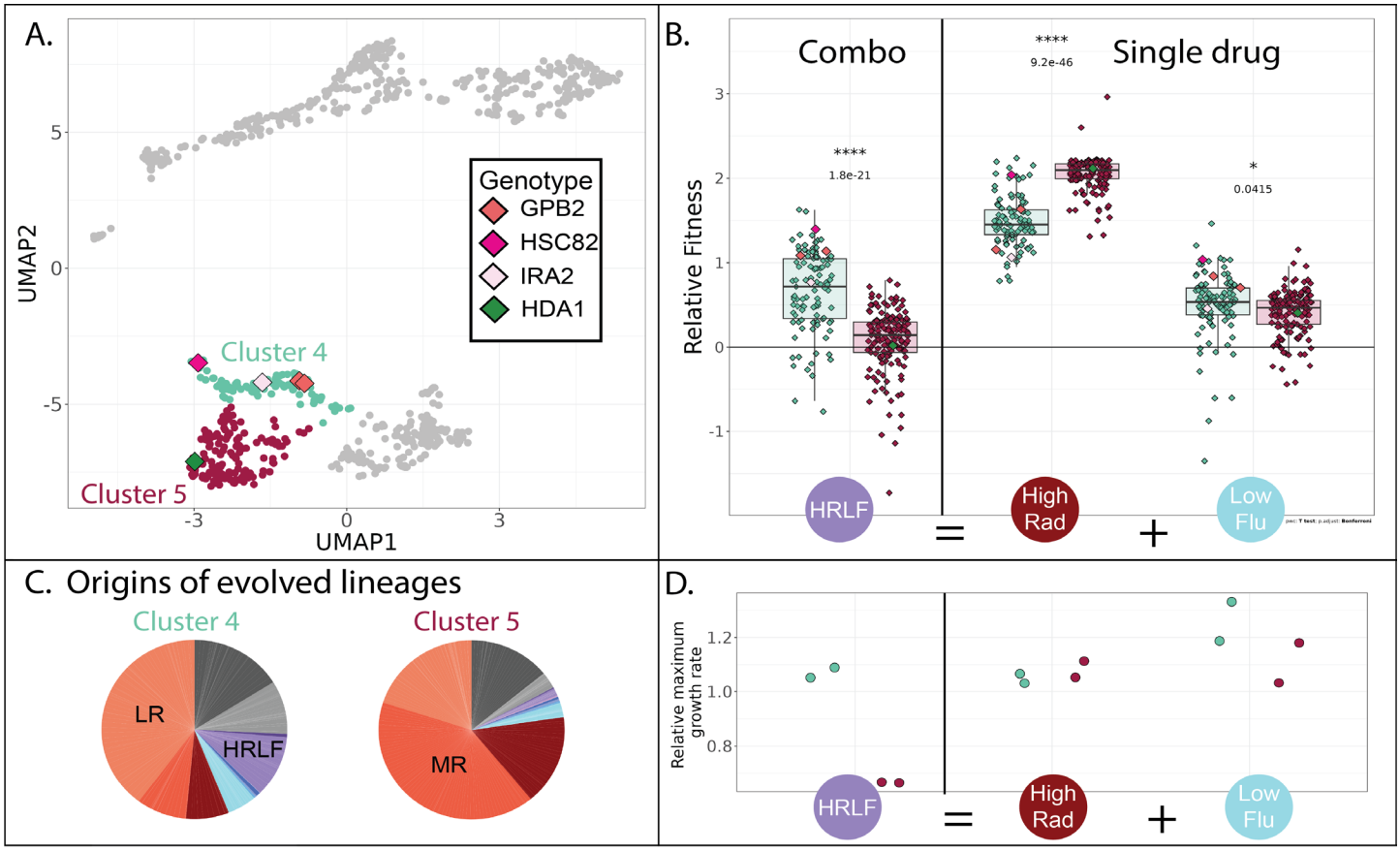

Figure 6: Evolved lineages in cluster 4 and 5 differ in response to combined drugs. (**A**) Adjacent clusters 4 and 5 each contain a small number of sequenced isolates depicted as diamonds; diamond colors corresponding to the genes containing adaptive mutations in each isolate. (**B**) Cluster 5 (red) has an unexpected fitness disadvantage in the HRLF multidrug environment relative to cluster 4 (green), given that cluster 5 lineages do not have a fitness disadvantage in the relevant single drug environments. Boxplots summarize the distribution across all lineages within each cluster in each environment, displaying the median (center line), interquartile range (IQR) (upper and lower hinges), and highest value within 1.5 × IQR (whiskers). (**C**) Pie charts display the relative frequency with which lineages in each cluster were sampled from each of the 12 evolution conditions, colors match those in table 1. (**D**) The maximum exponential growth rate for a single lineage isolated from each of clusters 4 (green) and 5 (red), relative to the ancestor. The growth rate of each lineage in each condition was measured twice by measuring changes in optical density over time. Tested lineage from cluster 4 has a mutation to GBP2 (S317T) while the lineage from cluster 5 has mutation to HDA1 (S600S).

to have reduced fitness in conditions containing neither FLU nor RAD as compared to cluster 2 lineages (**Figure 5B**). In sum, the differences between lineages in clusters 2 and 3 were not resolved upon normalizing fitness profiles to reduce magnitude differences, instead they were made more apparent (**Figure 5**). These differences do not appear to be random because they persist across experiments. For example, cluster 3 mutants are more fit in both medium and high RAD environments (**Figure 5B**; line plot) and were more often isolated from evolutions containing RAD (**Figure 5B**; pie charts). These observations beg a question: how can different mutations to the same gene affect fitness via different molecular mechanisms?

Asking this question forces us to consider what we mean by "mechanism." The mechanism by which mutations to PDR1 and PDR3 affect FLU resistance is well established: they increase transcription of an efflux pump that removes FLU from cells (Moye-Rowley 2019; Buechel and Pinkett 2020; Osset-Trénor et al. 2023). But if this is the only molecular-level effect of mutations to these genes, it is difficult to reconcile why PDR mutants fall into two distinct clusters with differently shaped fitness profiles. Others have also recently observed that mutants to PDR1 do not all behave the same way when exposed to novel drugs or changes in pH (Chen et al. 2023). This phenomenon is not reserved to PDR mutants, as adaptive missense mutations to another gene, IRA1, also do not share similarly shaped fitness profiles either (Kinsler et al. 2020). One explanation may be that, while all adaptive mutations within the same gene improve fitness via the same mechanism, not all mutants suffer the same costs. For example, perhaps the adaptive PDR mutations in cluster 2 cause misfolding of the PDR protein, resulting in lower fitness in RAD because this drug inhibits a chaperone that helps proteins to fold. In this case, it might be more correct to say that each of our six clusters affects fitness through a different, but potentially overlapping, suite of mechanisms (Wang et al. 2023). Previous work demonstrating that mutations commonly affect multiple traits supports this broader view of the mechanistic differences between clusters (Paaby and Rockman 2013; Boyle et al. 2017; Geiler-Samerotte et al. 2020; Kinsler et al. 2020).

Alternatively, perhaps not all adaptive mutations to PDR improve fitness via the same mechanism. PDR1 and PDR3 regulate transcription of YOR1 and SNQ2 as well as PDR5, and maybe the different clusters we observe represent mutants that upregulate one of these downstream targets more than the other (Osset-Trénor et al. 2023). Or, the mutants in each cluster might harbor different aneuploidies

bioRxiv preprint doi: https://doi.org/10.1101/2023.10.17.562616; this version posted October 20, 2023. The copyright holder for this preprint (which was not certified by peer review) is the author/funder, who has granted bioRxiv a license to display the preprint in perpetuity. It is made available under aCC-BY-ND 4.0 International license.

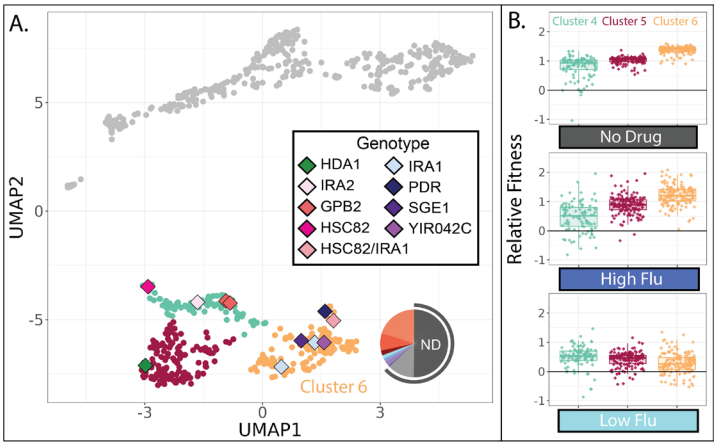

Figure 7: Evolved lineages in cluster 6 have higher fitness than other lineages in the absence of FLU and RAD. (**A**) Same UMAP as Figure 3D with clusters 4, 5, and 6 highlighted and sequenced isolates in these clusters represented as diamonds. Diamond colors correspond to the targets of adaptation in the sequenced isolates. Pie charts display the relative frequency with which lineages in cluster 6 were sampled from each of the 12 evolution conditions; colors match those in table 1. (**B**) Of the three clusters on the bottom half of the UMAP, cluster 6 lineages perform best in conditions without any drug and in the highest concentration of FLU. Yet they perform worst in the lowest concentration of FLU. Boxplots summarize the distribution across all lineages within each cluster in each environment, displaying the median (center line), interquartile range (IQR) (upper and lower hinges), and highest value within 1.5 × IQR (whiskers).

or small, difficult to sequence chromosomal insertions or deletions that affect fitness. We leave identification of the precise mechanisms that differentiate these clusters for future work. Here, using the example of PDR mutants, we showcase how genotype may not predict fitness tradeoffs, suggesting there is more to learn about the mechanisms underlying FLU resistance.

One group of RAD resistant mutants does not respond as expected to drug combinations

Though the three clusters of mutants on the bottom half of the UMAP are all advantageous in RAD and in conditions without any drug (**Figure 3E**; lower three plots), they differ in their fitness in conditions containing FLU. For example, the cluster of yeast lineages highlighted in green (cluster 4 in **Figures 3** & **6A**) is unique in that it has a slight advantage in the HRLF environment (**Figure 6B**). We found it especially strange that the neighboring cluster 5 does not also have a fitness advantage in this condition. Mutants in cluster 5 have a slight advantage in the LF condition, and a big advantage in the high RAD condition, thus we expect them to have at least some fitness advantage in the condition where these two drugs are combined (HRLF), but they do not (**Figure 6B**). The same is true for the combination of LRLF: cluster 5 mutants have an advantage in both single drug conditions which is lost when the drugs are combined (**Figure S10**). However, the mutants in cluster 4 (green) exhibit no such sensitivity to combined treatment. They have a slight advantage in all of the aforementioned single drug conditions, which is preserved in the relevant multidrug conditions (**Figure 6B** & **Figure S10**). To obtain an independent measure of the fitness of cluster 4 vs. cluster 5 lineages in these multidrug conditions, we asked from where the lineages in each cluster originate. About 10% of cluster 4 lineages originated from the HRLF evolution, while almost none of the lineages in cluster 5 came from this experiment, confirming that cluster 5 lineages are uniquely sensitive to this multidrug environment (**Figure 6C**).

The different fitness profiles of mutants in cluster 4 versus 5 (**Figure 6B** & **Figure S10**) might imply that they affect different phenotypes that ultimately underlie their drug resistance. We performed a follow-up experiment that supports this observation. We asked whether there are differences in the growth phenotypes of cluster 4 versus 5 mutants by measuring a growth curve for the lineage we were able to isolate from cluster 5, comparing it to a growth curve from a cluster 4 lineage (**Figure 6D**). Indeed, mutants in cluster 4 and 5 appear to have different growth curves in the relevant conditions (**Figure S10**). The growth differences echo those we see in the fitness data. For example, mutants in cluster 5 have a lower maximum growth rate in the HRLF multidrug condition, corresponding with their lower fitness in this condition relative to mutants in cluster 4 (**Figure 6B** & **6D**). However, the pattern reverses in the single drug conditions, both in terms of the fitness and growth data. These results suggest that the fitness differences we capture that differentiate these clusters are derived from differences in growth phenotypes.

One group of RAD resistant mutants is exceptionally adaptive in conditions without drug

One group of mutants in the lower half of the UMAP (cluster 6 in **Figure 7A**) appears distinct from the other two in that it has the largest fitness advantage in conditions lacking any drug (**Figure 7B**). This might imply that cluster 6 lineages rose to high frequency during our evolution experiments in environments without either drug, specifically the “no drug” and “DMSO” control conditions. Indeed, this is what we observe: over 50% of the lineages in cluster 6 were sampled from one of these two evolution experiments (**Figure 7A**). On the contrary, the other clusters in the lower half of the UMAP consist mainly of lineages sampled from one of the RAD evolutions (**Figure 6C**). Since our fitness experiments were performed independently of the evolution experiments, this provides two independent pieces of evidence suggesting that lineages in cluster 6 perform best in conditions lacking any drug.

In line with the success of cluster 6 mutants in no drug conditions, the five sequenced mutants in this cluster include three that have mutations to IRA1, which was the most common target of adaptation in another evolution experiment in the conditions we call “no drug” (**Figure 7A**) (Venkataram et al. 2016). In that experiment, and in ours, mutations to IRA1 result in a greater fitness advantage than mutations to its paralog, IRA2, or mutations to other negative regulators of the RAS/PKA pathway such as GPB2 (**Figure 7A**). Previous work showed that sometimes IRA1 mutants have very strong tradeoffs, for example, they become extremely maladaptive in environments containing salt or benomyl (Kinsler et al. 2020). We do not observe this to be the case for either FLU or RAD. In fact, we observe that cluster 6 mutants, including those in IRA1, maintain a fitness advantage in our highest concentration of both drugs (**Figure 3**), being more fit in high

bioRxiv preprint doi: https://doi.org/10.1101/2023.10.17.562616; this version posted October 20, 2023. The copyright holder for this preprint (which was not certified by peer review) is the author/funder, who has granted bioRxiv a license to display the preprint in perpetuity. It is made available under aCC-BY-ND 4.0 International license.

FLU than mutants in either of the other clusters in the lower half of the UMAP (**Figure 7B**). However, cluster 6 mutants are unique in that they lose their fitness advantage in the lowest concentration of FLU (**Figure 7B**). Being singularly sensitive to a low concentration of drug seems unusual, so much so that when this was observed previously for IRA1 mutants the authors added a note about the possibility of a technical error (Kinsler et al. 2020). Our results suggest that there is indeed something uniquely treacherous about the low fluconazole environment, at least for some genotypes.

Discussion:

Here, we present a barcoded collection of fluconazole (FLU) resistant yeast strains that is unique in its size, its diversity, and its tractability. One way we were able to isolate diverse types of FLU-resistance was by evolving yeast to resist diverse drug concentrations and combinations. But the more important tool used to increase both the number and type of mutants in our collection was DNA barcodes. These allowed us to sample beyond the drug resistant mutants that rise to appreciable frequency and to collect mutants that would eventually have been outcompeted by others. Our primary goal in collecting these mutants was to get a rough sense of how many different mechanisms of FLU resistance may exist. This question is relevant to evolutionary medicine (because more mechanisms of resistance make it harder to design strategies to avoid resistance), evolutionary theory (because more mechanisms of adaptation make it harder to predict how evolution will proceed), and genotype-phenotype mapping (because more mechanisms makes it more difficult to map which ones are associated with which mutations).

We distinguish mutants that act via different mechanisms by identifying those with different fitness tradeoffs across 12 environments, leveraging the mutants' barcodes to track their relative fitness following previous work (Kinsler et al. 2020). The 774 FLU-resistant mutants studied here clustered into a handful of groups (6) with characteristic tradeoffs. Some groupings are unintuitive in that they segregate mutations within the same gene (**Figure 5**) or are distinguished by unexpectedly low fitness in multidrug conditions (**Figure 6**). These findings are important because they challenge strategies in evolutionary medicine that rely on consistent tradeoffs or intuitive trends when designing sequential drug treatments. On the other hand, the observation that some mutants have very similar tradeoffs such that they cluster together is promising in that it suggests predicting the impact of some mutations by understanding the impacts of others may be feasible. Overall, our findings shed light on the degree of tractability in the genotype-phenotype map while emphasizing the need for enumerating classes of mutants before making predictions about the evolution of drug resistance.

Problematically, it is unclear to what extent it is possible to enumerate classes of mutant that resist a given drug. The six classes we present are incomplete and bound to change as additional data presents itself. For one, we have shown that additional FLU-resistant mutants emerge from evolution experiments in conditions lacking FLU (**Figure 2C** & **2D**). This begs questions about what other FLU-resistant mutants might emerge in environments we have not studied here. Additionally, previous work has shown that some mutants that group together in our study (e.g., GPB2 and IRA2) have different fitness profiles in conditions that we did not include here (Kinsler et al. 2020). Also of note is that our evolution experiments were conducted for only a few generations and all started from the same genetic background. Additional types of FLU-resistant mutants with unique fitness profiles may emerge from other genetic backgrounds or arise after more mutations are allowed to accumulate (Brandis et al. 2012; Bosch et al. 2021; Allen et al. 2021). Finally, by requiring that all included mutants have sufficient sequencing coverage in all 12 environments, our study is underpowered to detect adaptive lineages that have low fitness in any of the 12 environments. This is bound to exclude large numbers of adaptive mutants. For example, previous work has shown some FLU resistant mutants have strong tradeoffs in RAD (Cowen and Lindquist 2005). Perhaps we are unable to detect these mutants because their barcodes are at too low a frequency in RAD environments, thus they are excluded from our collection of 774. All of the aforementioned observations combined suggest that there are more unique types of FLU-resistant mutations than those represented by these 6 clusters, and that the molecular mechanisms that can contribute to fitness in FLU are more diverse than we know.

On the up side, not every infection harbors all possible types of mutants. This might explain why strategies that exploit one or two common tradeoffs have mixed success in delaying or preventing the emergence of resistance (Amin et al. 2015; Kaiser 2017; Imamovic et al. 2018; Wang et al. 2019; Krishna et al. 2022; Nyhoegen and Uecker 2023; Waller et al. 2023). Our results encourage more complex strategies to thwart resistance (Iram et al. 2020), such as those that focus on advance screening to determine the resistance mechanisms that are present (Andersson et al. 2019a), or on cycling a larger number of drugs to exploit a larger number of tradeoffs (Yoshida et al. 2017; Thomas et al. 2022). Problematically, these strategies rely on knowledge about the diversity of mutants and tradeoffs that exist (or that can emerge) within an infectious population. While information about population heterogeneity, heteroresistance, and substructure is expensive and arduous to obtain (Andersson et al. 2019b; Bottery et al. 2021), new methods, in addition to the one presented in this study, are emerging (Kuchina et al. 2021; Aissa et al. 2021; Nagasawa et al. 2021; Forsyth et al. 2021; Hsieh et al. 2022; Brettner et al. 2022a). This type of richer data dovetails with emerging population genetic models that predict the likelihood of resistance to a given drug regimen (Read and Huijben 2009; Day et al. 2015; Wilson et al. 2016; Cannataro et al. 2018; Somarelli et al. 2020; Feder et al. 2021; King et al. 2022). In short, our observation of numerous different types of drug-resistant mutations suggests that designing resistance-detering therapies is challenging, but perhaps not impossible.

Outside of predicting the evolution of resistance, our findings provide a tool to investigate the phenotypic impacts of mutation. This task has proven daunting in light of work

bioRxiv preprint doi: https://doi.org/10.1101/2023.10.17.562616; this version posted October 20, 2023. The copyright holder for this preprint (which was not certified by peer review) is the author/funder, who has granted bioRxiv a license to display the preprint in perpetuity. It is made available under aCC-BY-ND 4.0 International license.

demonstrating that mutations often have many phenotypic impacts (Paaby and Rockman 2013; Boyle et al. 2017) and that these impacts change with contexts including the environment (Paaby et al. 2015; Geiler-Samerotte et al. 2016, 2020; Lee et al. 2019; Eguchi et al. 2019). The approach presented in this study provides a way forward, not only by identifying mutations that likely affect similar phenotypes given their similar fitness tradeoffs, but also by identifying environments that differentiate one group of mutants from another. This suggests where to look to understand the different phenotypic impacts of each group of mutants. For example, we were able to show that the growth phenotypes of mutants from clusters 4 and 5 are different because we knew in which environments their fitness is different (**Figure 6**). Similarly, our results suggest radicicol environments may be helpful in teasing out any phenotypic differences that set apart some PDR mutations from others (**Figure 5**). In sum, our approach guides efforts to understand the phenotypic effects of mutation, while also guiding efforts to predict the effects of some mutations from others and to predict the outcomes of evolution.

Acknowledgements:
We are grateful to Sasha Levy for providing plasmids and yeast strains, to Martin Mullis, Xianan Liu, Sasha Levy and Gavin Sherlock for advice about creating a high diversity library of barcoded yeast, Jamie Blundell, Sandeep Venkataram and Fangfei Li for discussions about how to infer adaptive lineages, and to the members of the Geiler-Samerotte lab as well as Michael Lynch for discussions about the manuscript. The authors acknowledge resources and support from the KE core facilities at Arizona State University.

Funding:
This work was supported by a National Institutes of Health grant R35GM133674 (to KGS), an Alfred P Sloan Research Fellowship in Computational and Molecular Evolutionary Biology grant FG-2021-15705 (to KGS), and a National Science Foundation Biological Integration Institution grant 2119963 (to KGS).

Methods:

Base yeast strains
All of the yeast lineages studied here originated from the same starting strain referred to as the "landing pad strain" (SHA185) in previous work (Levy et al. 2015). We transformed a barcode library into this strain as described below, creating a strain with the following genetic background: MATα, ura3Δ0, ybr209w::Gal-Cre-KanMX-1/2URA3-loxP-Barcode-1/2URA3-HygMX-lox66/71.

Base media
All experiments were conducted in "M3" media defined in the same study as the landing pad strain (Levy et al. 2015), which is a glucose-limited media lacking uracil. In our study, we supplemented this media with fluconazole, radicicol, or DMSO when appropriate.

Selecting drug concentrations
Our goal was to choose concentrations of each drug that would not kill so many yeast cells as to dramatically decrease barcode diversity. We wanted to maintain a high number of unique barcodes so we could track a high number of yeast lineages as they independently evolved drug resistance. We measured the effect of each drug and drug combination on the growth rate of a single barcoded yeast strain using a plate reader to track changes in optical density (OD) over time. Ultimately we chose a "low" concentration of each drug that appeared to have no effect on growth rate, and a "high" concentration that appeared to reduce growth rate by about 15% (**Figure S2**). Though the lowest concentration of radicicol that we tested on a plate reader was 10 μM, we chose 5 μM as our low RAD concentration because previous work suggested this concentration had widespread effects on yeast physiology without affecting growth (Jarosz and Lindquist 2010; Geiler-Samerotte et al. 2016). To perform our plate reader experiment, a single colony was grown to saturation. From this culture, 5 μl was added to every well of a 96-well plate, where every well contained 195 μl of M3 media. Some wells also contained either fluconazole, radicicol, DMSO, or combinations of these drugs. The concentrations that were tested are listed on the horizontal axis of **figure S2**; each drug condition was replicated six times. The 96-well plate was incubated at 30°C for 48 hours on a plate reader and OD measurements were taken every 30 minutes. Raw OD values were exported and maximum exponential growth rates for all tested conditions were calculated from the log-linear changes in OD over time.

Inserting 300,000 unique DNA barcodes into otherwise genetically identical yeast cells
In order to track many yeast lineages as they independently develop drug resistance, we needed to insert unique DNA barcodes into many yeast cells. Plasmids harboring barcodes (pBar3) were the same as those used in a previous barcoded evolution experiment (Levy et al. 2015) and were generously provided to us by Sasha Levy. These barcodes are 25 base pairs in length. They are targeted to an artificial intron within the Ura3 gene, such that they must be retained in media lacking uracil but are not expressed and thus do not themselves affect fitness (Levy et al. 2015). We transformed this barcode library (pBar3) into the landing pad strain (SHA185) as was done previously, activating a Cre-lox recombination system by growing the cells in YP-galactose, which resulted in genomic integration of the barcode. However, our efforts to perform extremely high efficiency transformations from which we could isolate hundreds of thousands of uniquely barcoded yeast were unsuccessful, despite manipulating the levels and timing of the inducer (galactose). Ultimately we performed 24 separate transformations and pooled many of these to obtain a large pool of barcoded yeast where every yeast cell was genetically identical except for its DNA barcode.

Examining the frequency of each barcode in the starting pool of cells
We sequenced each of these 24 transformed yeast populations on the Hiseq X platform using a dual index system (Kinsler et al. 2023) to discern barcode coverage, i.e., how many total unique barcodes were successfully inserted into yeast cells and how evenly these barcodes were sampled. We needed

bioRxiv preprint doi: https://doi.org/10.1101/2023.10.17.562616; this version posted October 20, 2023. The copyright holder for this preprint (which was not certified by peer review) is the author/funder, who has granted bioRxiv a license to display the preprint in perpetuity. It is made available under aCC-BY-ND 4.0 International license.

many uniquely barcoded yeast in order to observe many different adaptive lineages within each evolution experiment. But barcodes with very high frequencies, referred to herein as monster lineages, were present in 10 of the 24 transformations and present a problem. Monster lineages allow too many cells to carry the same barcode, giving that barcode more chances to develop an adaptive mutation. This could allow different cells harboring that same barcode to pick up different adaptive mutations, destroying our ability to draw conclusions about adaptive mutations by using barcodes. Therefore, our final library of barcoded lineages was created by pooling 14 individual transformations together, choosing those 14 that lacked monster lineages, which we defined as lineages representing greater than 1% of all transformants. Our sequencing results suggest that this library contains about 300,000 unique barcodes.

Initiating 12 barcoded evolution experiments

All evolution experiments started from the same pool of roughly 300,000 uniquely barcoded yeast lineages. To start the evolution experiments, a pea sized amount of the frozen yeast barcode library was grown up in 4 ml YPD for 4 hours at 30 °C in a shaking incubator at 220 rpm. Then, 300 μl of the grown barcode library was added to each of 12 pre-prepared 500mL flasks representing the 12 evolution experiments listed in **Table 1**. To prepare these flasks, first, 1.2 L of M3 media was warmed at 30°C. Then, 100 ml was added to each of 12 flat bottom flasks. Next, 500 μl of the appropriate drug or drug combination was added to each flask. Drugs were pre-diluted, aliquoted and frozen such that 500 μl of the appropriate tube could be added to each flask to achieve the desired concentration as listed in **Table 1**. All drugs were resuspended in DMSO such that the final concentration of DMSO in all experiments (except the “no drug” control) was 0.5%.

Performing barcoded evolution experiments

Evolution experiments were performed following previous work (Levy et al. 2015). After initiation (see above), the yeast in every flask were allowed to grow at 30°C with shaking at 200 RPM for 48 hours. Then, the flasks were removed from the incubator and 400 – 1000 μl of each culture was transferred to a new pre-prepared flask with identical conditions to the first. The reason we added more volume (1000 μl) to some flasks than previous work was that the cell counts at the end of the 48 hours were lower for some of our higher drug conditions. We adjusted the transfer volume to maintain a transfer population of 4x107 cells, which was the same as in previous work (Levy et al. 2015). We completed a total of 24 growth/transfer cycles, corresponding to 192 generations of growth assuming 8 generations per 48-hour cycle (Levy et al. 2015). Following each transfer, the remaining culture from each flask were split into two 50 ml conical vials, centrifuged for 3 minutes at 4000 rpm, and the supernatant was discarded. The final pellet was resuspended in 30% glycerol up to a total volume of 6 ml before being split into three 2 ml cryovials and stored at -80°C. These frozen samples were later utilized for barcode sequencing and isolating adaptive mutants.

Isolating a large pool of adaptive mutants

We performed evolution experiments in order to generate a large pool of diverse adaptive mutants. Our goal was to collect a sample from each evolution experiment at a time point when there were many different adaptive lineages competing. If we sampled too late, the adaptive lineage with the greatest fitness advantage would have already risen to high frequency, thus reducing diversity. But if we sampled too early, adaptive lineages would not yet have risen in frequency above other lineages. Therefore, we chose to sample cells from a time in each evolution experiment when many barcoded lineages appeared to be rising in frequency (**Figure S1**). We sampled either 1 or 2 thousand cells per each evolution experiment by spreading frozen stock from the chosen time point onto agarose plates, scraping 1 or 2 thousand colonies into a 15mL conical tube containing a final concentration of 30% glycerol, and freezing the pool pertaining to each of the 12 evolutions. We sampled 2,000 cells from most evolution experiments, but sampled only 1,000 from those containing a high concentration of FLU as those evolutions appeared to have reduced barcoded diversity (**Figure S1**), presumably because high FLU represents a strong selective pressure. We sequenced the barcodes from each of these 12 pools so that we could track which adaptive mutants originated from which evolution experiment (see methods section below entitled, “Inferring where adaptive lineages originally evolved”).

Initiating barcoded fitness competition experiments

To assess the fitnesses of the 1 or 2 thousand barcoded lineages that we sampled from each evolution experiment, we pooled all sampled lineages together into a larger pool of roughly 21,000 barcoded lineages. We used this larger pool to initiate 24 fitness competition experiments, 2 replicates for each of the 12 conditions listed in **Table 1**. In this type of competition, we measure fitness by tracking changes in each barcode’s frequency over time. Barcodes that rise in frequency represent strains that have higher fitness than others.

Our goal was to calculate the fitness effect of adaptive mutations. Therefore, we needed to calculate the fitness of every evolved lineage relative to the unmutated ancestor of the evolution experiments. To do so, we followed previous work by spiking in a large quantity of this unmutated ancestor strain into each fitness competition, with this ancestor making up at least 90% of the final culture (Venkataram et al. 2016; Kinsler et al. 2020). In environments containing a high concentration of FLU which resulted in the ancestral strain having a more severe growth defect, we spiked in the ancestor such that it represented 95% of the final pool.

To avoid wasting 90% or more of our sequencing reads on the ancestor strain’s barcode, we created a barcodeless ancestor strain. This strain was created by transforming SHA185 with a linear piece of DNA such that the genetic background was identical to the strains of the barcoded library, but the homology to the primers used to amplify the barcode was missing. Thus the DNA from these cells does not get amplified or sequenced during subsequent steps.

In addition to this barcodeless ancestor, we also spiked in

bioRxiv preprint doi: https://doi.org/10.1101/2023.10.17.562616; this version posted October 20, 2023. The copyright holder for this preprint (which was not certified by peer review) is the author/funder, who has granted bioRxiv a license to display the preprint in perpetuity. It is made available under aCC-BY-ND 4.0 International license.

some barcoded ancestral strains at lower frequency (1%) to use as "reference" or "control" strains, following previous work (Kinsler et al. 2020, 2023). These strains have been previously shown to possess no fitness differences from the ancestor. We used these strains as a baseline when calculating relative fitness by setting the fitness of these strains to zero during our fitness inference procedure (see methods section below entitled, "Inferring fitness").

All 24 fitness competitions were performed simultaneously in one big batch (Kinsler et al. 2023) and initiated from the same pool of roughly 21,000 barcoded evolved yeast lineages, barcodeless ancestor, and control strains. To initiate the competitions, 7x107 cells from this pool were added to 24 pre-prepared 500mL flasks corresponding to the conditions listed in **Table 1**. These flasks were prepared exactly the same way as was done for the evolution experiments (see above in "Performing barcoded evolution experiments"). Each flask was allowed to grow for 48 hours at 30°C with shaking at 200 RPM.

Performing barcoded fitness competition experiments

Fitness competitions were performed following previous work (Kinsler et al. 2020). After the initial flasks were allowed to grow for 48 hours, they were removed from the incubator and 4x107 cells from each culture representing 400 µl were transferred to a new flask with identical media. For each of 24 competitions, we completed a total of 4 growth/transfer cycles, corresponding to 40 generations of growth assuming 8 generations per 48-hour cycle (Levy et al. 2015). Following each transfer, the remaining culture from each flask was split into two 50 ml conical vials, centrifuged for 3 minutes at 4000 rpm, and the supernatant was discarded. The final pellet was resuspended in 30% glycerol up to a total volume of 6 ml before being split into three 2 ml cryovials and stored at -80°C. These frozen samples were later utilized for DNA extraction and subsequent barcode sequencing.

Extracting genomic DNA

DNA was extracted from 500 µl of concentrated frozen stocks pertaining to the evolution experiments and fitness competitions. Frozen cells were thawed and pelleted. Cells were treated with 250 µl of 0.1 M Na2EDTA, 1M sorbitol and 5U/µl zymolyase for a minimum of 15 minutes at 37 °C to remove the cell wall. Lysis was completed by adding 250 µl of 1% SDS, 0.2N NaOH and inverting to mix. Proteins and cell debris were removed with 5M KOAc by spinning for 5 min at 15,000 rpm. Supernatant was moved to a new tube and DNA was precipitated with 600 µl isopropanol by spinning for 5 min at 15,000 rpm. The resulting pellet was washed 1 ml of 70% ethanol before being resuspended in 50 µl water plus 10µg/ml RNAse. Extracted DNA was quantified using the NanoDrop spectrophotometer and all samples were diluted to a concentration of 50 ng/μL for barcode amplification and sequencing library preparation.

Preparing barcodes for high-throughput multiplexed sequencing using PCR

Extracted DNA was prepared for sequencing using a two-step PCR that preserves information about the relative frequency of each barcode in each sample (Venkataram et al. 2016; Kinsler et al. 2020, 2023). Briefly, in the first step PCR, the barcode region is amplified from the genomic DNA, labeled with a sample-specific combination of primers, and tagged with a UMI. This step utilizes a short 3 cycle PCR with New England Biolabs OneTaq polymerase. Purification of the first step product to remove excess reagents was performed using Thermo Scientific GeneJET PCR Purification Kit. The second step PCR attached Illumina indices that were used to distinguish samples from different experiments and timepoints. We utilized a dual indexing scheme to prevent index misassignment that is common when sequencing amplicon libraries using patterned flow cell technology (Kinsler et al. 2023). Amplification of this second step of PCR was done with a longer 23 cycle PCR using Q5 polymerase. Final libraries were bead purified using 0.8X Quantabio sparQ Pure Mag beads. Quantification of the final PCR products was done using the Invitrogen Qubit Fluorometer before all samples were pooled at equimolar ratios for sequencing.

Sequencing and clustering barcodes

Next Generation Sequencing was performed at either Psomagen (Rockville, MD) or at the Translation Genomics Research Institute (Phoenix, AZ) on patterned flow cells (either an Illumina HiSeqX or NovaSeq) using 2 x 150 base pair paired end reads. Samples were dual indexed to allow multiplexing while minimizing contamination from index misassignments (Kinsler et al. 2023). The 20 base pairs of variable sequence referred to as a DNA barcode were identified and clustered to determine the number of unique barcodes and the frequency of each barcode in each sample. For the evolution experiments, this was done following our previous work (Venkataram et al. 2016; Kinsler et al. 2020). For the fitness competition experiments, this was done using updated software (Zhao et al. 2018) with the following command:

```
bartender_extractor_com -f ${SAMPLE}_R1_001.fastq -o ${SAMPLE}_extracted -q 0 -p GTACC[5]AA[5]AA[5]TT[5]ATAAC -m 2 -d f -u 0,8
```

Inferring fitness

In fitness competition experiments, fitness is often inferred from the log-linear change in a strain's frequency over time (Geiler-Samerotte et al. 2011; Bakerlee et al. 2021; Kinsler et al. 2023). Recently, more advanced methods to infer fitness have emerged that take into account nonlinearities in frequency changes over time, for example, nonlinearities that reflect changes in the mean fitness of the population (Venkataram et al. 2016; Li et al. 2018a, 2023; Kinsler et al. 2020). We had trouble implementing these newer methods on our fitness data, perhaps because many of our evolved lineages, and our control strains, have low fitness in some drugs. This caused their barcodes to rapidly decline in frequency such that they received low counts only at later time points. Their counts could become so low that these lineages would seemingly disappear due to sampling error, and then reappear at a subsequent time point. This dramatic (but false) increase in frequency was sometimes interpreted as evidence of very high fitness, especially when we inferred fitness using approaches that account for nonlinearities.

bioRxiv preprint doi: https://doi.org/10.1101/2023.10.17.562616; this version posted October 20, 2023. The copyright holder for this preprint (which was not certified by peer review) is the author/funder, who has granted bioRxiv a license to display the preprint in perpetuity. It is made available under aCC-BY-ND 4.0 International license.

To contend with this issue, we applied strict coverage thresholds to every fitness measurement: we required at least 500 counts across all timepoints in order to infer fitness for a given lineage in a given environment. This is stricter than previous work that does not require a minimum number of reads per fitness measurement and instead thresholds on the average coverage per lineage per time point (Kinsler et al. 2020). We found that 774 lineages passed our threshold in at least one replicate experiment per all 12 environments. Of these, 729 passed for both replicates and the final fitness value we report represents the average of both replicates.

Even with our strict coverage threshold, some fitness inference methods still interpreted minor stochastic fluctuations in fitness at later time points as evidence of a fitness advantage, even if fitness dramatically declined in earlier time points. Therefore, we calculated fitness via the traditional method, as the slope of the log-linear change in barcode frequency relative to the average slope of the control strains, as this method is less sensitive to that type of error. Using this method, we found that our fitness inferences were reproducible between replicates (**Figure S4A**), and between experiments performed in similar conditions (e.g., medium vs. high concentrations of the same drug) (**Figure S4B**). When we increased our coverage threshold to require an order of magnitude more reads per lineage per measurement (from 500 to 5000), we lost 157 lineages (from 774 to 617), saw reproducibility increase across replicates (from an average Pearson correlation of 0.756 to 0.813) and the main conclusions of our study were unchanged in that the same 6 clusters were present on a UMAP (**Figure S7**).

Identifying adaptive mutations using whole-genome sequencing

One downside of barcoded evolution experiments is that all lineages exist together in a pooled culture. Fishing out adaptive lineages in order to perform whole genome sequencing is a major challenge (Venkataram et al. 2016). Here, we randomly selected cells from these mixed pools for whole genome sequencing, sometimes selecting from later time points in the evolution experiments and sometimes selecting from the samples of 1 or 2 thousand cells that were isolated to initiate fitness competitions.

To perform whole genome sequencing, cells from mixed pools were spread onto M3 agarose plates, single colonies were selected and grown in YPD to saturation. DNA was extracted using the PureLink™ Genomic DNA Mini Kit (K182002). Sequencing libraries were made using Illumina DNA Prep kit by diluting reactions by 1/5. Briefly, samples were prepared such that the starting concentration in 6 ul was between 20 and 100 ng of DNA. 2µl of BLT and TB1were added to the starting material and incubated on a thermocycler at 55°C (lid 100°C) for 15 min. 2 µl of TSB was added to each reaction and incubated at 37 C (lid 100°C) for 15 min. Beads were washed 2 times with 20 µl of TWB. Following the final wash, 4 µl of EPM, 4 µl of water and 2 µl of UD indexes were added to each sample. Depending on starting concentration, PCR was performed based on Illumina guidelines as follows: lid 100°C, 68°C for 3 min, 98C for 3 min, [98°C for 45s, 62°C for 30s, 68°C for 2min] for 6 to 10 cycles, 68°C for 1 min, 10°C hold. PCR products were cleaned with a double side sized selection as follows: 4 µl of each sample was pooled together (32 µl total for 8 samples) and added to 28 µl of water plus 32 µl of SPB. After a 5 min incubation 25 µl of supernatant was moved to a new tube containing 3 µl of SPB. Beads were washed with fresh 80% ethanol and libraries were eluted in 12 µl RSB. Samples were multiplexed using Illumina's unique dual (UD) index plates (A-D) and sequencing was performed with 2x150 paired end sequencing on HiSeq X at Psomagen (Rockville, MD).

In total 122 colonies were randomly picked and sequenced. As one might expect, barcodes that rose to high frequency were more likely to be picked multiple times. In an attempt to avoid this and find lineages with unique attributes, some cultures were grown at 37°C or plated to high concentrations of drug prior to picking isolated colonies for sequencing. Of the 122 genomes we sequenced, only 53 pertained to the 774 lineages for which we obtained high enough barcode coverage to infer fitness. Only two of these 53 had no sequenced mutations suggesting its fitness increase over ancestor is due to a change in ploidy. The other 51 all had at least one single nucleotide mutation in a gene reported in **supplemental table 1**.

Variant calling was done using GATK as described here: https://github.com/gencorefacility/variant-calling-pipeline-gatk4. Identified variants were annotated using SnpEff (Cingolani et al. 2012). Variant call files from 132 (53 unique/in CS) sequenced lineages were analyzed in R and compared to reference strain GCF_000146045.2 (Genome assembly 64: sacCer3). SNPs present in the ancestor (as well as all evolved lineages) were ignored as these could not have caused the fitness differences we observed. We also ignored SNPS that were present in a substantial number of evolved lineages, as these likely represent background mutations that were present in a substantial portion of the cells representing the landing pad strain (SHA185). These are reported in **supplemental table 1** and include: SRD1-Glu97Lys, RSC30-Gly571Asp, OPT1-Val143Ile and LYS20-Thr29Met.

Measuring growth rates of evolved lineages with unexpected fitness in multidrug conditions

Though fitness differences are not necessarily due to differences in maximum growth rate (Li et al. 2018b), we measured growth curves for a few lineages to investigate a case where an evolved lineage had unexpectedly low fitness in multidrug conditions (**Figure 6B**). Indeed, we found that this mutant grew more slowly in those conditions. To perform this test, lineages with mutations to GBP2 and HDA1 as well the ancestor strain were streaked to YPD plates. We used the barcodeless ancestor strain, which is identical to the evolved lineages in every way except for lacking a barcode, and is described above in the methods section entitled, "Initiating barcoded fitness competition experiments". A single colony of each strain was isolated from YPD plates and was used to inoculate an overnight YPD culture. After ~24 hours, a coulter

bioRxiv preprint doi: https://doi.org/10.1101/2023.10.17.562616; this version posted October 20, 2023. The copyright holder for this preprint (which was not certified by peer review) is the author/funder, who has granted bioRxiv a license to display the preprint in perpetuity. It is made available under aCC-BY-ND 4.0 International license.

counter (BD) was used to determine the number of cells/ml present in each culture. Next,, all cultures were diluted such that the starting number of cells in each growth curve measurement was 250,000 in 6 ml of M3 plus drug (HR, LF and HRLF). To measure cell growth rates, these samples were allowed to grow at 30 degrees C. OD was measured every 10 minutes as the cultures were grown to saturation using the compact rocking incubator TVS062CA (Advantec Mfs). Raw growth curves for these conditions are shown in **Figure S10B**. Maximum growth rate was calculated using a sliding window approach to determine the region of each growth curve with the steepest log-linear slope.

Determining ploidy

While our barcoded yeast strain is haploid, previous studies observed that some cells diploidize during the course of evolution in M3 media and by doing so gain a fitness advantage (Levy et al. 2015; Venkataram et al. 2016). To ensure that observed fitness effects in our experiments were not largely due to the effects of diploids, we estimated the percent of diploid cells in each of our populations. We chose to make our estimates from frozen samples taken at the same time points from which we sampled 1 or 2 thousand cells to initiate fitness competitions (**Figure S1**). As such, our estimates also report on the percent of diploids that were present at the start of the fitness competitions experiments (**Table S2**).

To study ploidy, we used the nucleic acid stain SYTOX Green, which is capable of selectively staining the nucleus of fixed cells and has been shown to be more optimal for use in budding yeast than the standard propidium iodide stain (Haase 2004). For each of the 12 evolution experiments conditions, a small amount of freezer stock from the chosen timepoints (**Figure S1**) was plated to YPD and grown for ~48 hours. Individual colonies were picked and transferred to 96-well plates, 1 full plate for each condition, before being fixed with 95% ethanol for 1 hour. Plates were centrifuged at 4500 rpm and supernatant was discarded. 50 µL RNase A was added to the samples at a concentration of 2mg/mL, and the plates were then incubated for 2 hours at 37°C. Cells were pelleted by centrifuge and the supernatant was removed, which was followed by treatment with 20 µL of the protease pepsin at a concentration of 5mg/uL. Pepsin treated samples incubated at 37°C for 30 minutes before centrifugation and removal of supernatant. Finally, cells were resuspended in 50 µL TrisCL (50 mM, pH 8) and stained with 100 µL of 1µM SYTOX Green. Known diploid and haploid strains were used as controls alongside our samples to determine the expected fluorescence of stained diploid vs. haploid cells. Analysis was performed using a ThermoFisher Attune NxT, housed in the Flow Cytometry Core Facility at Arizona State University.

Dimensional reduction

Our fitness inference procedure resulted in a data set consisting of nearly 10,000 fitness measurements (774 lineages x 12 conditions = 9288 fitness measurements). Dimensional reduction was performed on these data using UMAP (McInnes et al. 2018b). Clusters of similar mutants were identified and colored using a gaussian mixed model (Fraley and Raftery 2003); Bayesian Information Criteria were used to select the number of clusters (**Figure S6**). These analyses were performed in R; code can be found https://osf.io/pxyv9/?view_only=51241d8f00c24f7e83f1ece3ae31a53b.

In order to prevent conditions with the most variation in fitness (e.g., high FLU) from dominating, we normalized fitness measurements from each of the 12 environments to have the same overall mean and variance (we transformed the data from every environment to have a mean of 0 and a standard deviation of 1) before performing dimensional reduction. This normalization procedure did not have a dramatic effect on the UMAP (**Figure S7A**). We also explored normalizing all data to account for magnitude differences by setting the average fitness of each lineage across all 12 environments to 0. Doing so did not significantly change the groupings present in the UMAP from those displayed in **Figure 3** (**Figure S9**) other than in the ways we describe in Figure 5. Reducing our data set to 617 adaptive lineages with very high sequencing coverage (**Figure S7B**) also did not significantly affect the way that mutants cluster into groups, nor did using a different dimensional reduction algorithm altogether (**Figure S8**). In short, the clustering of mutants was robust to the different decisions we made when choosing how to analyze these data.

In order to assess whether clusters identified from the UMAP are robust to alternative clustering methods, we also used hierarchical clustering to identify clusters of mutants with similar fitness profiles. First, we computed the pairwise distance of all lineages across the fitness profiles. Then, we used Ward's method from scikit-learn to iteratively cluster lineages such that the within-cluster variation is minimized (Ward 1963; Pedregosa et al. 2012). To test the consistency of lineage clustering, we chose a pairwise cluster distance cutoff of 11, which results in the same number of clusters (7) as identified with the UMAP clustering approach used in the main text. We then compared the identity of the lineages within each of these clusters with the UMAP clusters. We found that, for most clusters, over 80% of lineages from the UMAP cluster corresponded with a unique hierarchical cluster and labeled these hierarchical clusters according to this correspondence (**Figure S8**). For UMAP cluster 1, lineages were more evenly split between two clusters. 64% of these lineages clustered together in what is labeled as hierarchical cluster 1 and 30% in hierarchical cluster 1/7 (**Figure S8**), which contains all of the control lineages that comprise UMAP cluster 7. Despite these lineages clustering more closely with control lineages than the remainder of the cluster 1, they do tend to cluster distinctly with the control lineages, suggesting they have behavior that is distinguishable from the control lineages. If we consider these cluster 1 mutants that end up in cluster 3/7 as "mis-clustered", we find that 85% of lineages from each UMAP cluster are clustered together in the corresponding hierarchical cluster. If we consider these as "consistently clustered", this metric increases to 90% of lineages correctly clustered. Altogether, this analysis shows that the results we show are robust to alternative methods of clustering.

bioRxiv preprint doi: https://doi.org/10.1101/2023.10.17.562616; this version posted October 20, 2023. The copyright holder for this preprint (which was not certified by peer review) is the author/funder, who has granted bioRxiv a license to display the preprint in perpetuity. It is made available under aCC-BY-ND 4.0 International license.

Inferring where adaptive lineages originally evolved

All 774 adaptive lineages were isolated from one of the 12 evolution experiments at the timepoint indicated in f**igure S1** (see Methods section entitled, "Isolating a large pool of adaptive mutants"). The sample we isolated from each evolution experiment was sequenced prior to pooling. This allows us to computationally determine which barcoded lineages originated from which evolution experiment to generate the pie charts in **Figures 2, 4, 5, 6** and **7**.

If adaptive mutation arose independently during the course of each evolution experiment, it would be unlikely for any adaptive lineage we study to be present in more than one of the evolution conditions. This would make it very easy to assign each barcode to the evolution experiment from which it originated. However, this was not the case for many barcoded lineages.

Previous work explained that the transformation procedure used to insert a barcode into the landing pad of SHA185 was itself mutagenic, such that many of the mutations arose prior to the start of the evolution experiments (Levy et al. 2015). Since all our evolution experiments were started from the same pool of barcoded lineages, we thus expect that many adaptive lineages will be present in more than one condition. However, it is not expected that these adaptive lineages will be present at the same frequency in every condition; instead these frequencies change with the fitness of the mutation each lineage possesses. Therefore, when an adaptive lineage appeared in multiple conditions, we weighted its origin to reflect its frequency in each condition. In other words, adaptive lineages that were only present in the sample taken from a single evolution condition were identified and assigned a single origin condition in the pie charts in **Figures 2, 4, 5,6,** and **7**. But for adaptive lineages found in the samples taken from more than one evolution condition, the proportions assigned to each origin condition in the pie charts was scaled to equal the relative frequencies of that lineage in all evolution conditions where it was observed. Associated data and code can be found here: https://osf.io/pxyv9/?view_only=51241d8f00c24f7e83f1ece3ae31a53b.

References

1. Abel zur Wiesch P, Kouyos R, Abel S, et al (2014) Cycling empirical antibiotic therapy in hospitals: meta-analysis and models. PLoS Pathog 10:e1004225
2. Aissa AF, Islam ABMMK, Ariss MM, et al (2021) Single-cell transcriptional changes associated with drug tolerance and response to combination therapies in cancer. Nat Commun 12:1628
3. Algazi AP, Othus M, Daud AI, et al (2020) Continuous versus intermittent BRAF and MEK inhibition in patients with BRAF-mutated melanoma: a randomized phase 2 trial. Nat Med 26:1564–1568
4. Allen RC, Angst DC, Hall AR (2019) Resistance Gene Carriage Predicts Growth of Natural and Clinical Escherichia coli Isolates in the Absence of Antibiotics. Appl Environ Microbiol 85.: https://doi.org/10.1128/AEM.02111-18
5. Allen RC, Pfrunder-Cardozo KR, Hall AR (2021) Collateral Sensitivity Interactions between Antibiotics Depend on Local Abiotic Conditions. mSystems 6:e0105521
6. Amin AD, Rajan SS, Liang WS, et al (2015) Evidence Suggesting That Discontinuous Dosing of ALK Kinase Inhibitors May Prolong Control of ALK+ Tumors. Cancer Res 75:2916–2927
7. Andersson DI, Hughes D (2010) Antibiotic resistance and its cost: is it possible to reverse resistance? Nat Rev Microbiol 8:260–271
8. Andersson DI, Nicoloff H, Hjort K (2019a) Mechanisms and clinical relevance of bacterial heteroresistance. Nat Rev Microbiol 17:479–496
9. Andersson DI, Nicoloff H, Hjort K (2019b) Mechanisms and clinical relevance of bacterial heteroresistance. Nat Rev Microbiol 17:479–496
10. Ardell SM, Kryazhimskiy S (2021) The population genetics of collateral resistance and sensitivity. Elife 10.: https://doi.org/10.7554/eLife.73250
11. Baker CM, Ferrari MJ, Shea K (2018) Beyond dose: Pulsed antibiotic treatment schedules can maintain individual benefit while reducing resistance. Sci Rep 8:5866
12. Bakerlee CW, Phillips AM, Nguyen Ba AN, Desai MM (2021) Dynamics and variability in the pleiotropic effects of adaptation in laboratory budding yeast populations. Elife 10.: https://doi.org/10.7554/eLife.70918
13. Basra P, Alsaadi A, Bernal-Astrain G, et al (2018) Fitness Tradeoffs of Antibiotic Resistance in Extraintestinal Pathogenic Escherichia coli. Genome Biol Evol 10:667–679
14. Baym M, Stone LK, Kishony R (2016) Multidrug evolutionary strategies to reverse antibiotic resistance. Science 351:aad3292
15. Berkow E, Lockhart S (2017) Fluconazole resistance in Candida species: a current perspective. Infection and Drug Resistance 10:237–245
16. Berman J, Krysan DJ (2020) Drug resistance and tolerance in fungi. Nat Rev Microbiol 18:319–331
17. Bongomin F, Gago S, Oladele RO, Denning DW (2017) Global and Multi-National Prevalence of Fungal Diseases-Estimate Precision. J Fungi (Basel) 3.: https://doi.org/10.3390/jof3040057
18. Bosch B, DeJesus MA, Poulton NC, et al (2021) Genome-wide gene expression tuning reveals diverse vulnerabilities of M. tuberculosis. Cell 184:4579–4592.e24
19. Bottery MJ, Pitchford JW, Friman V-P (2021) Ecology and evolution of antimicrobial resistance in bacterial communities. ISME J 15:939–948
20. Boyer S, Hérissant L, Sherlock G (2021) Adaptation is influenced by the complexity of environmental change during evolution in a dynamic environment. PLoS Genet 17:e1009314
21. Boyle EA, Li YI, Pritchard JK (2017) An Expanded View of Complex Traits: From Polygenic to Omnigenic. Cell 169:1177–1186
22. Brandis G, Wrande M, Liljas L, Hughes D (2012) Fitness-

bioRxiv preprint doi: https://doi.org/10.1101/2023.10.17.562616; this version posted October 20, 2023. The copyright holder for this preprint (which was not certified by peer review) is the author/funder, who has granted bioRxiv a license to display the preprint in perpetuity. It is made available under aCC-BY-ND 4.0 International license.

compensatory mutations in rifampicin-resistant RNA polymerase. Mol Microbiol 85:142–151
23. Brettner L, Eder R, Schmidlin K, Geiler-Samerotte K (2022a) An ultra high-throughput, massively multiplexable, single-cell RNA-seq platform in yeasts. bioRxiv 2022.09.12.507686
24. Brettner L, Ho WC, Schmidlin K, Apodaca S (2022b) Challenges and potential solutions for studying the genetic and phenotypic architecture of adaptation in microbes. Current Opinion in
25. Buechel ER, Pinkett HW (2020) Transcription factors and ABC transporters: from pleiotropic drug resistance to cellular signaling in yeast. FEBS Lett 594:3943–3964
26. Cairns J, Borse F, Mononen T, et al (2022) Strong selective environments determine evolutionary outcome in time-dependent fitness seascapes. Evol Lett 6:266–279
27. Cannataro VL, Gaffney SG, Stender C, et al (2018) Heterogeneity and mutation in KRAS and associated oncogenes: evaluating the potential for the evolution of resistance to targeting of KRAS G12C. Oncogene 37:2444–2455
28. Centers for Disease Control and Prevention (U.S.) (2019) Antibiotic Resistance Threats in the United States, 2019. U.S. Department of Health and Human Services, Centres for Disease Control and Prevention
29. Chen VK, Johnson MS, Hérissant L, et al (2023) Far From Home: Evolution of haploid and diploid populations reveals common, strong, and variable pleiotropic effects in non-home environments. bioRxiv 2023.02.28.530341
30. Cingolani P, Platts A, Wang LL, et al (2012) A program for annotating and predicting the effects of single nucleotide polymorphisms, SnpEff: SNPs in the genome of Drosophila melanogaster strain w1118; iso-2; iso-3. Fly 6:80–92
31. Cowen LE, Lindquist S (2005) Hsp90 potentiates the rapid evolution of new traits: drug resistance in diverse fungi. Science 309:2185–2189
32. Cowen LE, Sanglard D, Howard SJ, et al (2014) Mechanisms of Antifungal Drug Resistance. Cold Spring Harb Perspect Med 5:a019752
33. Cowen LE, Singh SD, Köhler JR, et al (2009) Harnessing Hsp90 function as a powerful, broadly effective therapeutic strategy for fungal infectious disease. Proc Natl Acad Sci U S A 106:2818–2823
34. Day T, Huijben S, Read AF (2015) Is selection relevant in the evolutionary emergence of drug resistance? Trends Microbiol 23:126–133
35. Eguchi Y, Bilolikar G, Geiler-Samerotte K (2019) Why and how to study genetic changes with context-dependent effects. Curr Opin Genet Dev 58-59:95–102
36. Fardeau V, Lelandais G, Oldfield A, et al (2007) The Central Role of PDR1 in the Foundation of Yeast Drug Resistance*. J Biol Chem 282:5063–5074
37. Feder AF, Harper KN, Brumme CJ, Pennings PS (2021) Understanding patterns of HIV multi-drug resistance through models of temporal and spatial drug heterogeneity. Elife 10.: https://doi.org/10.7554/eLife.69032
38. Flowers SA, Barker KS, Berkow EL, et al (2012) Gain-of-function mutations in UPC2 are a frequent cause of ERG11 upregulation in azole-resistant clinical isolates of Candida albicans. Eukaryot Cell 11:1289–1299
39. Forsyth B, Torab P, Lee J-H, et al (2021) A Rapid Single-Cell Antimicrobial Susceptibility Testing Workflow for Bloodstream Infections. Biosensors 11.: https://doi.org/10.3390/bios11080288
40. Fraley C, Raftery AE (2003) Enhanced Model-Based Clustering, Density Estimation,and Discriminant Analysis Software: MCLUST. J Classification 20:263–286
41. Geiler-Samerotte KA, Dion MF, Budnik BA, et al (2011) Misfolded proteins impose a dosage-dependent fitness cost and trigger a cytosolic unfolded protein response in yeast. Proc Natl Acad Sci U S A 108:680–685
42. Geiler-Samerotte KA, Li S, Lazaris C, et al (2020) Extent and context dependence of pleiotropy revealed by high-throughput single-cell phenotyping. PLoS Biol 18:e3000836
43. Geiler-Samerotte KA, Zhu YO, Goulet BE, et al (2016) Selection Transforms the Landscape of Genetic Variation Interacting with Hsp90. PLoS Biol 14:e2000465
44. Gjini E, Wood KB (2021) Price equation captures the role of drug interactions and collateral effects in the evolution of multidrug resistance. Elife 10.: https://doi.org/10.7554/eLife.64851
45. Gomulkiewicz R, Kirkpatrick M (1992) QUANTITATIVE GENETICS AND THE EVOLUTION OF REACTION NORMS. Evolution 46:390–411
46. Good BH, McDonald MJ, Barrick JE, et al (2017) The dynamics of molecular evolution over 60,000 generations. Nature 551:45–50
47. Grier HE, Krailo MD, Tarbell NJ, et al (2003) Addition of ifosfamide and etoposide to standard chemotherapy for Ewing's sarcoma and primitive neuroectodermal tumor of bone. N Engl J Med 348:694–701
48. Haase SB (2004) Cell cycle analysis of budding yeast using SYTOX Green. Curr Protoc Cytom Chapter 7:Unit 7.23
49. Hall MD, Handley MD, Gottesman MM (2009) Is resistance useless? Multidrug resistance and collateral sensitivity. Trends Pharmacol Sci 30:546–556
50. Harris A, Wagner M, Du D, et al (2021) Structure and efflux mechanism of the yeast pleiotropic drug resistance transporter Pdr5. Nat Commun 12:5254
51. Herren CM, Baym M (2022) Decreased thermal niche breadth as a trade-off of antibiotic resistance. ISME J 16:1843–1852
52. Hill JA, O'Meara TR, Cowen LE (2015) Fitness Trade-Offs Associated with the Evolution of Resistance to Antifungal Drug Combinations. Cell Rep 10:809–819
53. Hsieh K, Mach KE, Zhang P, et al (2022) Combating Antimicrobial Resistance via Single-Cell Diagnostic Technologies Powered by Droplet Microfluidics. Acc Chem Res 55:123–133
54. Imamovic L, Ellabaan MMH, Dantas Machado AM, et al (2018) Drug-Driven Phenotypic Convergence Supports Rational Treatment Strategies of Chronic Infections. Cell 172:121–134.e14
55. Iram S, Dolson E, Chiel J, et al (2020) Controlling the speed and trajectory of evolution with counterdiabatic

bioRxiv preprint doi: https://doi.org/10.1101/2023.10.17.562616; this version posted October 20, 2023. The copyright holder for this preprint (which was not certified by peer review) is the author/funder, who has granted bioRxiv a license to display the preprint in perpetuity. It is made available under aCC-BY-ND 4.0 International license.

driving. Nat Phys 17:135–142
56. Iwasawa J, Maeda T, Shibai A, et al (2022) Analysis of the evolution of resistance to multiple antibiotics enables prediction of the Escherichia coli phenotype-based fitness landscape. PLoS Biol 20:e3001920
57. Iyer KR, Robbins N, Cowen LE (2022) The role of Candida albicans stress response pathways in antifungal tolerance and resistance. iScience 25:103953
58. Jarosz DF, Lindquist S (2010) Hsp90 and Environmental Stress Transform the Adaptive Value of Natural Genetic Variation. Science 330:1820–1824
59. Jerison ER, Nguyen Ba AN, Desai MM, Kryazhimskiy S (2020) Chance and necessity in the pleiotropic consequences of adaptation for budding yeast. Nat Ecol Evol 4:601–611
60. Kaiser J (2017) When less is more. Science 355:1144–1146
61. Kapitzky L, Beltrao P, Berens TJ, et al (2010) Cross-species chemogenomic profiling reveals evolutionarily conserved drug mode of action. Mol Syst Biol 6:451
62. King ES, Maltas J, Weaver DT, et al (2022) Fitness seascapes are necessary for realistic modeling of the evolutionary response to drug therapy. biorxiv
63. Kinsler G, Geiler-Samerotte K, Petrov DA (2020) Fitness variation across subtle environmental perturbations reveals local modularity and global pleiotropy of adaptation. Elife 9.: https://doi.org/10.7554/eLife.61271
64. Kinsler G, Schmidlin K, Newell D, et al (2023) Extreme sensitivity of fitness to environmental conditions: Lessons from #1BigBatch. J Mol Evol 91:293–310
65. Kolaczkowski M, van der Rest M, Cybularz-Kolaczkowska A, et al (1996) Anticancer drugs, ionophoric peptides, and steroids as substrates of the yeast multidrug transporter Pdr5p. J Biol Chem 271:31543–31548
66. Krishna A, Zere T, Mistry S, et al (2022) Evaluation of a Sequential Antibiotic Treatment Regimen of Ampicillin, Ciprofloxacin and Fosfomycin against Escherichia coli CFT073 in the Hollow Fiber Infection Model Compared with Simultaneous Combination Treatment. Antibiotics (Basel) 11.: https://doi.org/10.3390/antibiotics11121705
67. Ksiezopolska E, Schikora-Tamarit MÀ, Beyer R, et al (2021) Narrow mutational signatures drive acquisition of multidrug resistance in the fungal pathogen Candida glabrata. Curr Biol 31:5314–5326.e10
68. Kuchina A, Brettner LM, Paleologu L, et al (2021) Microbial single-cell RNA sequencing by split-pool barcoding. Science 371.: https://doi.org/10.1126/science.aba5257
69. Larkins-Ford J, Degefu YN, Van N, et al (2022) Design principles to assemble drug combinations for effective tuberculosis therapy using interpretable pairwise drug response measurements. Cell Rep Med 3:100737
70. Lässig M, Mustonen V, Walczak AM (2017) Predicting evolution. Nat Ecol Evol 1:77
71. Lee JT, Coradini ALV, Shen A, Ehrenreich IM (2019) Layers of Cryptic Genetic Variation Underlie a Yeast Complex Trait. Genetics 211:1469–1482
72. Levy SF, Blundell JR, Venkataram S, et al (2015) Quantitative evolutionary dynamics using high-resolution lineage tracking. Nature 519:181–186
73. Li F, Salit ML, Levy SF (2018a) Unbiased Fitness Estimation of Pooled Barcode or Amplicon Sequencing Studies. Cell Syst 7:521–525.e4
74. Li F, Tarkington J, Sherlock G (2023) Fit-Seq2.0: An Improved Software for High-Throughput Fitness Measurements Using Pooled Competition Assays. J Mol Evol 91:334–344
75. Li Y, Petrov DA, Sherlock G (2019) Single nucleotide mapping of trait space reveals Pareto fronts that constrain adaptation. Nat Ecol Evol 3:1539–1551
76. Li Y, Venkataram S, Agarwala A, et al (2018b) Hidden Complexity of Yeast Adaptation under Simple Evolutionary Conditions. Curr Biol 28:515–525.e6
77. Logan A, Wolfe A, Williamson JC (2022) Antifungal Resistance and the Role of New Therapeutic Agents. Curr Infect Dis Rep 24:105–116
78. Lupetti A, Danesi R, Campa M, et al (2002) Molecular basis of resistance to azole antifungals. Trends Mol Med 8:76–81
79. Maltas J, Wood KB (2019) Pervasive and diverse collateral sensitivity profiles inform optimal strategies to limit antibiotic resistance. PLoS Biol 17:e3000515
80. Martínez AA, Lang GI (2023) Identifying Targets of Selection in Laboratory Evolution Experiments. J Mol Evol. https://doi.org/10.1007/s00239-023-10096-2
81. McInnes L, Healy J, Melville J (2018a) UMAP: Uniform Manifold Approximation and Projection for Dimension Reduction. arXiv [stat.ML]
82. McInnes L, Healy J, Saul N, Großberger L (2018b) UMAP: Uniform Manifold Approximation and Projection. J Open Source Softw 3:861
83. Melnikov SV, Stevens DL, Fu X, et al (2020) Exploiting evolutionary trade-offs for posttreatment management of drug-resistant populations. Proc Natl Acad Sci U S A 117:17924–17931
84. Mira PM, Crona K, Greene D, et al (2015) Rational design of antibiotic treatment plans: a treatment strategy for managing evolution and reversing resistance. PLoS One 10:e0122283
85. Mirkin B (2011) Choosing the number of clusters. Wiley Interdiscip Rev Data Min Knowl Discov 1:252–260
86. Miyazaki H, Miyazaki Y, Geber A, et al (1998) Fluconazole resistance associated with drug efflux and increased transcription of a drug transporter gene, PDH1, in Candida glabrata. Antimicrob Agents Chemother 42:1695–1701
87. Moye-Rowley WS (2019) Multiple interfaces control activity of the Candida glabrata Pdr1 transcription factor mediating azole drug resistance. Curr Genet 65:103–108
88. Nagasawa S, Kashima Y, Suzuki A, Suzuki Y (2021) Single-cell and spatial analyses of cancer cells: toward elucidating the molecular mechanisms of clonal evolution and drug resistance acquisition. Inflamm Regen 41:22
89. Nichol D, Rutter J, Bryant C, et al (2019) Antibiotic collateral sensitivity is contingent on the repeatability of evolution. Nat Commun 10:334
90. Nyhoegen C, Uecker H (2023) Sequential antibiotic therapy in the laboratory and in the patient. J R Soc Interface 20:20220793
91. Ogbunugafor CB (2022) The mutation effect reaction norm (mu-rn) highlights environmentally dependent mutation effects and epistatic interactions. Evolution

bioRxiv preprint doi: https://doi.org/10.1101/2023.10.17.562616; this version posted October 20, 2023. The copyright holder for this preprint (which was not certified by peer review) is the author/funder, who has granted bioRxiv a license to display the preprint in perpetuity. It is made available under aCC-BY-ND 4.0 International license.

76:37–48
92. Osset-Trénor P, Pascual-Ahuir A, Proft M (2023) Fungal Drug Response and Antimicrobial Resistance. J Fungi (Basel) 9.: https://doi.org/10.3390/jof9050565
93. Paaby AB, Rockman MV (2013) The many faces of pleiotropy. Trends Genet 29:66–73
94. Paaby AB, White AG, Riccardi DD, et al (2015) Wild worm embryogenesis harbors ubiquitous polygenic modifier variation. Elife 4.: https://doi.org/10.7554/eLife.09178
95. Pál C, Papp B, Lázár V (2015) Collateral sensitivity of antibiotic-resistant microbes. Trends Microbiol 23:401–407
96. Palmer AC, Kishony R (2014) Opposing effects of target overexpression reveal drug mechanisms. Nat Commun 5:4296
97. Pedregosa F, Varoquaux G, Gramfort A, et al (2012) Scikit-learn: Machine Learning in Python. arXiv [cs.LG] 2825–2830
98. Petti S, Reddy G, Desai MM (2023) Inferring sparse structure in genotype-phenotype maps. Genetics. https://doi.org/10.1093/genetics/iyad127
99. Pinheiro F, Warsi O, Andersson DI, Lässig M (2021) Metabolic fitness landscapes predict the evolution of antibiotic resistance. Nat Ecol Evol 5:677–687
100. Raymond B (2019) Five rules for resistance management in the antibiotic apocalypse, a road map for integrated microbial management. Evol Appl 12:1079–1091
101. Read AF, Huijben S (2009) Evolutionary biology and the avoidance of antimicrobial resistance. Evol Appl 2:40–51
102. Robbins N, Leach MD, Cowen LE (2012) Lysine deacetylases Hda1 and Rpd3 regulate Hsp90 function thereby governing fungal drug resistance. Cell Rep 2:878–888
103. Rodrigues JV, Bershtein S, Li A, et al (2016) Biophysical principles predict fitness landscapes of drug resistance. Proc Natl Acad Sci U S A 113:E1470–8
104. Roemhild R, Linkevicius M, Andersson DI (2020) Molecular mechanisms of collateral sensitivity to the antibiotic nitrofurantoin. PLoS Biol 18:e3000612
105. Roe SM, Prodromou C, O'Brien R, et al (1999) Structural basis for inhibition of the Hsp90 molecular chaperone by the antitumor antibiotics radicicol and geldanamycin. J Med Chem 42:260–266
106. Rybak JM, Cuomo CA, Rogers PD (2022) The molecular and genetic basis of antifungal resistance in the emerging fungal pathogen Candida auris. Curr Opin Microbiol 70:102208
107. Scarborough JA, McClure E, Anderson P, et al (2020) Identifying States of Collateral Sensitivity during the Evolution of Therapeutic Resistance in Ewing's Sarcoma. iScience 23:101293
108. Schmidt F, Efferth T (2016) Tumor Heterogeneity, Single-Cell Sequencing, and Drug Resistance. Pharmaceuticals 9.: https://doi.org/10.3390/ph9020033
109. Somarelli JA, Gardner H, Cannataro VL, et al (2020) Molecular Biology and Evolution of Cancer: From Discovery to Action. Mol Biol Evol 37:320–326
110. Sorgo AG, Heilmann CJ, Dekker HL, et al (2011) Effects of fluconazole on the secretome, the wall proteome, and wall integrity of the clinical fungus Candida albicans. Eukaryot Cell 10:1071–1081
111. Su M, Satola SW, Read TD (2019) Genome-Based Prediction of Bacterial Antibiotic Resistance. J Clin Microbiol 57.: https://doi.org/10.1128/JCM.01405-18
112. Tanaka S, Tani M (2018) Mannosylinositol phosphorylceramides and ergosterol coodinately maintain cell wall integrity in the yeast Saccharomyces cerevisiae. FEBS J 285:2405–2427
113. Tan L, Chen L, Yang H, et al (2022) Structural basis for activation of fungal sterol receptor Upc2 and azole resistance. Nat Chem Biol 18:1253–1262
114. Tenaillon O, Rodríguez-Verdugo A, Gaut RL, et al (2012) The molecular diversity of adaptive convergence. Science 335:457–461
115. Thomas DS, Cisneros LH, Anderson ARA, Maley CC (2022) In Silico Investigations of Multi-Drug Adaptive Therapy Protocols. Cancers 14.: https://doi.org/10.3390/cancers14112699
116. Uemura S, Moriguchi T (2022) Pleiotropic roles of N-glycans for enzyme activities and stabilities of MIPC synthases, Csh1 and Sur1/Csg1, in Saccharomyces cerevisiae. Glycobiology 32:778–790
117. Vasicek EM, Berkow EL, Flowers SA, et al (2014) UPC2 is universally essential for azole antifungal resistance in Candida albicans. Eukaryot Cell 13:933–946
118. Venkataram S, Dunn B, Li Y, et al (2016) Development of a Comprehensive Genotype-to-Fitness Map of Adaptation-Driving Mutations in Yeast. Cell 166:1585–1596.e22
119. Ventola CL (2015) The antibiotic resistance crisis: part 1: causes and threats. P T 40:277–283
120. Vik Å, Rine J (2001) Upc2p and Ecm22p, dual regulators of sterol biosynthesis in Saccharomyces cerevisiae. Mol Cell Biol 21:6395–6405
121. Vu BG, Moye-Rowley WS (2022) Nonidentical function of Upc2A binding sites in the Candida glabrata CDR1 promoter. Genetics 222.: https://doi.org/10.1093/genetics/iyac135
122. Waller NJE, Cheung C-Y, Cook GM, McNeil MB (2023) The evolution of antibiotic resistance is associated with collateral drug phenotypes in Mycobacterium tuberculosis. Nat Commun 14:1517
123. Wang W-Y, Cai H-Q, Qu S-Y, et al (2022) Genomic Variation-Mediating Fluconazole Resistance in Yeast. Biomolecules 12.: https://doi.org/10.3390/biom12060845
124. Wang X, Zhang H, Chen X (2019) Drug resistance and combating drug resistance in cancer. Cancer Drug Resist 2:141–160
125. Wang Y, Sang M, Feng L, et al (2023) A pleiotropic–epistatic entangelement model of drug response. Drug Discov Today 103790
126. Ward JH (1963) Hierarchical Grouping to Optimize an Objective Function. J Am Stat Assoc 58:236–244
127. Whitesell L, Santagata S, Mendillo ML, et al (2014) HSP90 empowers evolution of resistance to hormonal therapy in human breast cancer models. Proc Natl Acad Sci U S A 111:18297–18302

bioRxiv preprint doi: https://doi.org/10.1101/2023.10.17.562616; this version posted October 20, 2023. The copyright holder for this preprint (which was not certified by peer review) is the author/funder, who has granted bioRxiv a license to display the preprint in perpetuity. It is made available under aCC-BY-ND 4.0 International license.

128. Wilson BA, Garud NR, Feder AF, et al (2016) The population genetics of drug resistance evolution in natural populations of viral, bacterial and eukaryotic pathogens. Mol Ecol 25:42–66
129. Wortel MT, Agashe D, Bailey SF, et al (2023) Towards evolutionary predictions: Current promises and challenges. Evol Appl 16:3–21
130. Xie JL, Polvi EJ, Shekhar-Guturja T, Cowen LE (2014) Elucidating drug resistance in human fungal pathogens. Future Microbiol 9:523–542
131. Yadav A, Radhakrishnan A, Bhanot G, Sinha H (2015) Differential regulation of antagonistic pleiotropy in synthetic and natural populations suggests its role in adaptation. G3 5:699–709
132. Yang F, Scopel EFC, Li H, et al (2023) Antifungal Tolerance and Resistance Emerge at Distinct Drug Concentrations and Rely upon Different Aneuploid Chromosomes. MBio 14:e0022723
133. Yoon N, Krishnan N, Scott J (2021) Theoretical modeling of collaterally sensitive drug cycles: shaping heterogeneity to allow adaptive therapy. J Math Biol 83:47
134. Yoshida M, Reyes SG, Tsuda S, et al (2017) Time-programmable drug dosing allows the manipulation, suppression and reversal of antibiotic drug resistance in vitro. Nat Commun 8:15589
135. Zhao L, Liu Z, Levy SF, Wu S (2018) Bartender: a fast and accurate clustering algorithm to count barcode reads. Bioinformatics 34:739–747
136. Zhao Q, Hautamaki V, Fränti P (2008) Knee Point Detection in BIC for Detecting the Number of Clusters. In: Advanced Concepts for Intelligent Vision Systems. Springer Berlin Heidelberg, pp 664–673

bioRxiv preprint doi: https://doi.org/10.1101/2023.10.17.562616; this version posted October 20, 2023. The copyright holder for this preprint (which was not certified by peer review) is the author/funder, who has granted bioRxiv a license to display the preprint in perpetuity. It is made available under aCC-BY-ND 4.0 International license.

Supplemental Figures and Tables

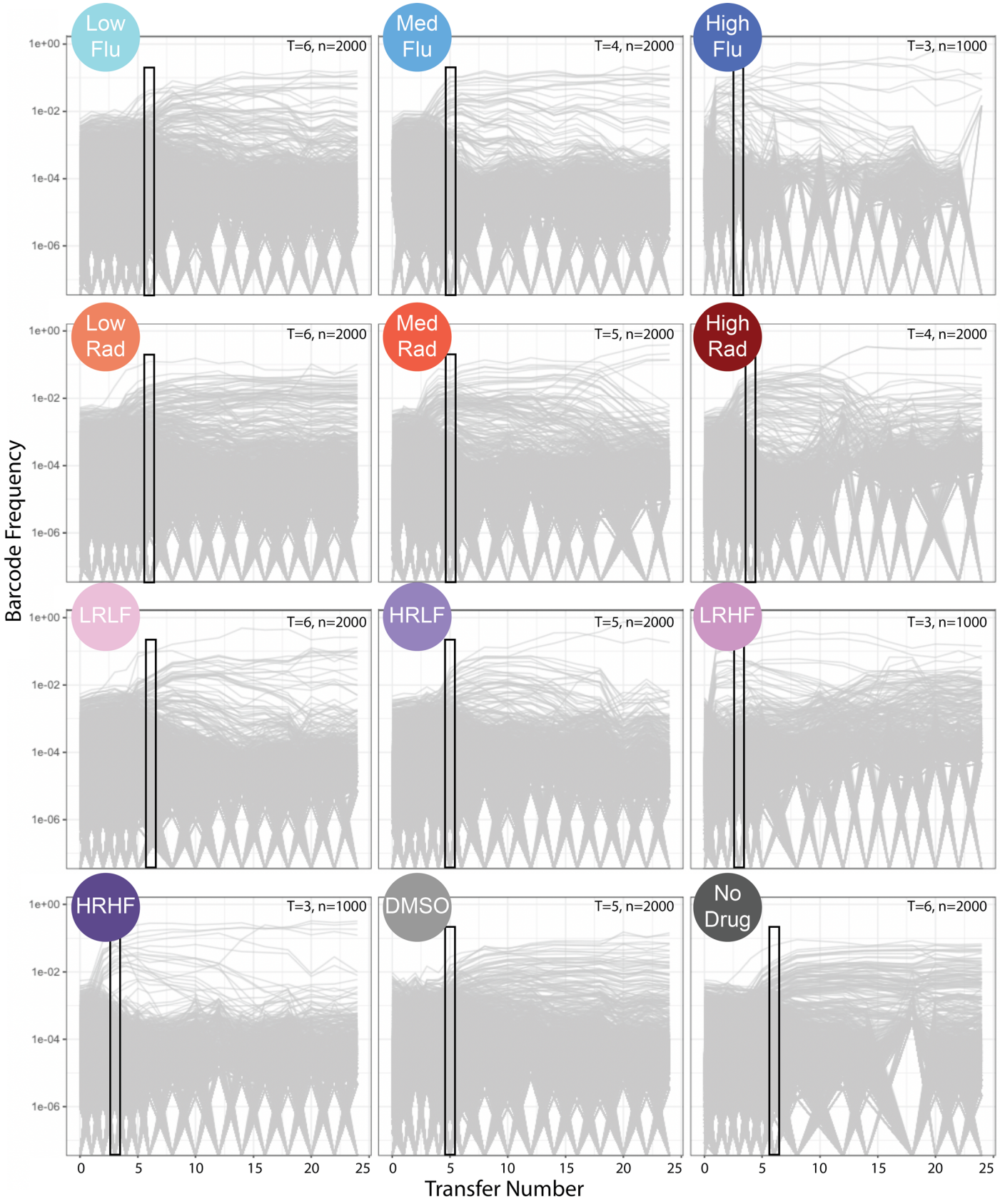

Figure S1: Twelve barcoded evolution experiments track ~300,000 lineages as they adapt to different drug concentrations and combinations. In each plot, every line represents a unique barcoded lineage. The vertical axis represents barcode frequency. When lineages reach a frequency of zero it means they were not sampled at that time point of the experiment. The black boxes indicate the transfer number of each evolution experiment from which evolved lineages are sampled; the number of cells sampled (colonies picked) is in the upper right hand corner.

bioRxiv preprint doi: https://doi.org/10.1101/2023.10.17.562616; this version posted October 20, 2023. The copyright holder for this preprint (which was not certified by peer review) is the author/funder, who has granted bioRxiv a license to display the preprint in perpetuity. It is made available under aCC-BY-ND 4.0 International license.

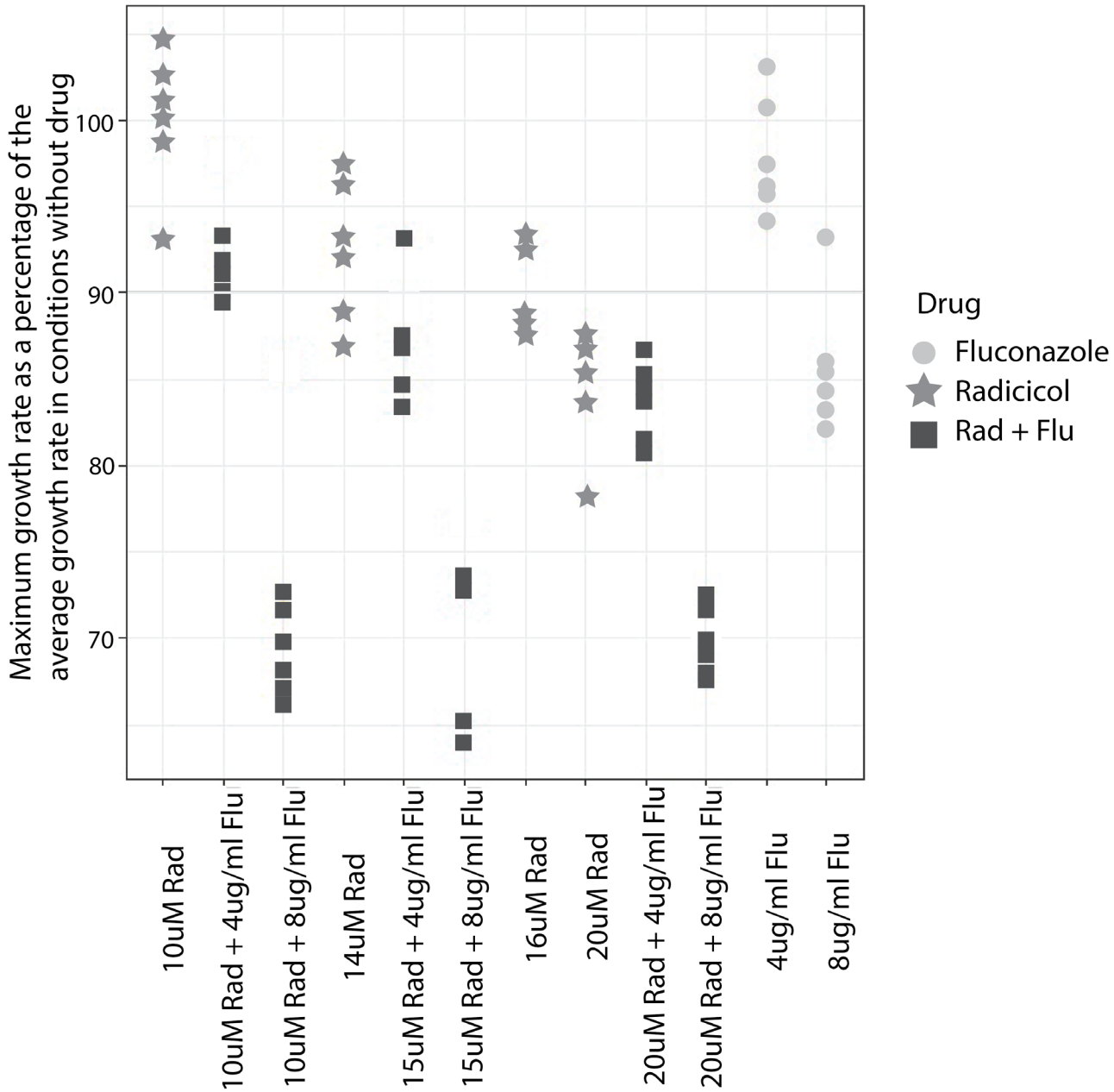

Figure S2: Chosen drug concentrations do not dramatically reduce yeast's maximum growth rate. We measured the growth rate of a single barcoded yeast lineage, prior to the evolution experiment, in different concentrations and combinations of drugs using a plate reader to track changes in optical density over time. Maximum growth rate is reported as a percentage of the maximum growth rate in conditions lacking FLU or RAD. Maximum growth rate was calculated as the maximum log-linear slope of the change in optical density over time.

bioRxiv preprint doi: https://doi.org/10.1101/2023.10.17.562616; this version posted October 20, 2023. The copyright holder for this preprint (which was not certified by peer review) is the author/funder, who has granted bioRxiv a license to display the preprint in perpetuity. It is made available under aCC-BY-ND 4.0 International license.

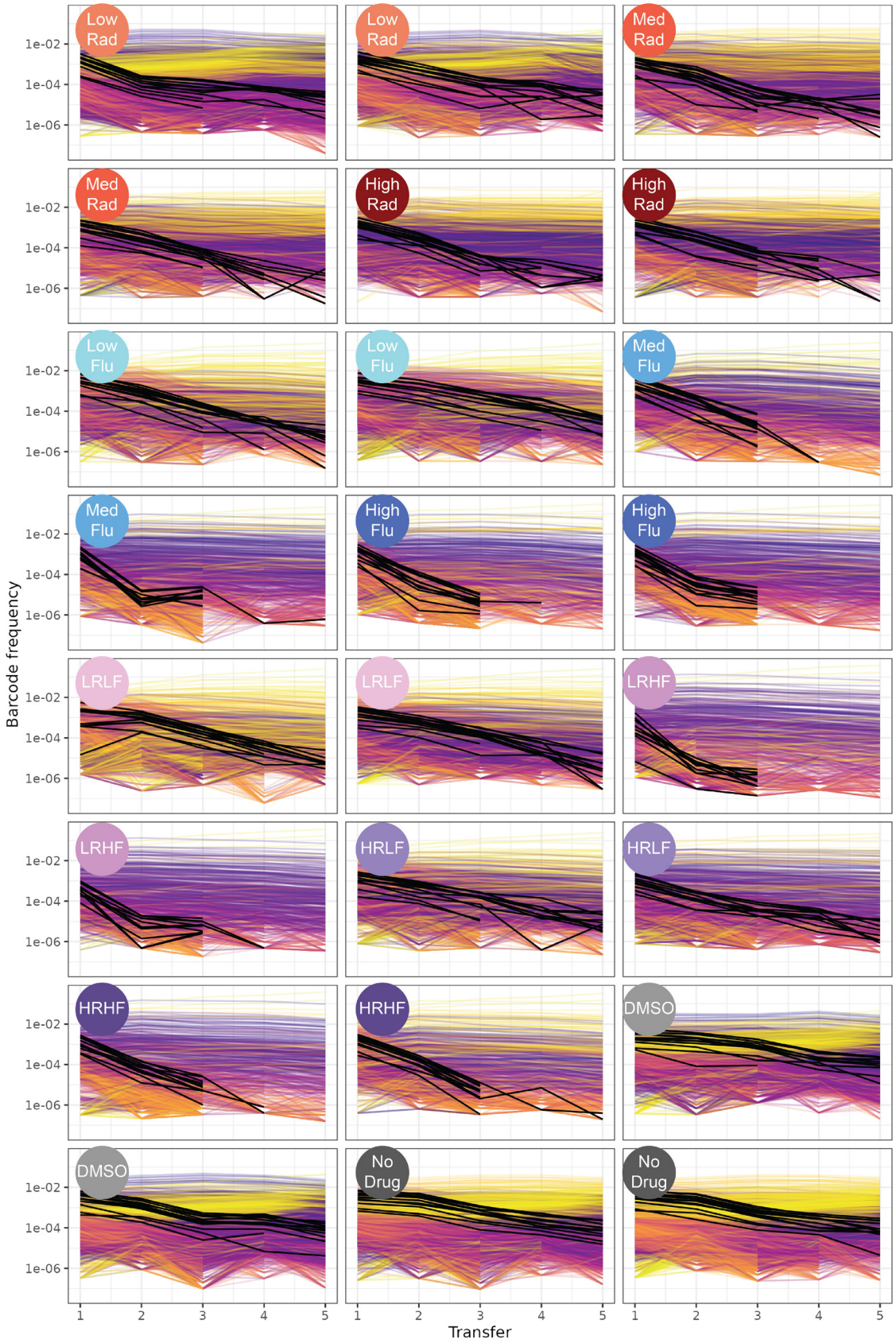

Figure S3: Twenty four fitness competitions track evolved lineages as their barcodes change frequency. In each plot, every line represents a barcoded lineage. Lineages with >5 reads per experiment are shown (4,815). Control lineages, known to possess no sequenced mutations from the ancestor, are highlighted in black. Evolved lineages with higher fitness than controls are yellow, similar fitness to controls (i.e., relative fitness ~0) are purple, and lower fitness than controls are orange. When a lineage declines in frequency so much that its associated barcode is no longer observed, its line abruptly ends. Some lineages appear to decline and then increase in frequency; this happens because low frequency lineages are subject to sampling noise.

bioRxiv preprint doi: https://doi.org/10.1101/2023.10.17.562616; this version posted October 20, 2023. The copyright holder for this preprint (which was not certified by peer review) is the author/funder, who has granted bioRxiv a license to display the preprint in perpetuity. It is made available under aCC-BY-ND 4.0 International license.

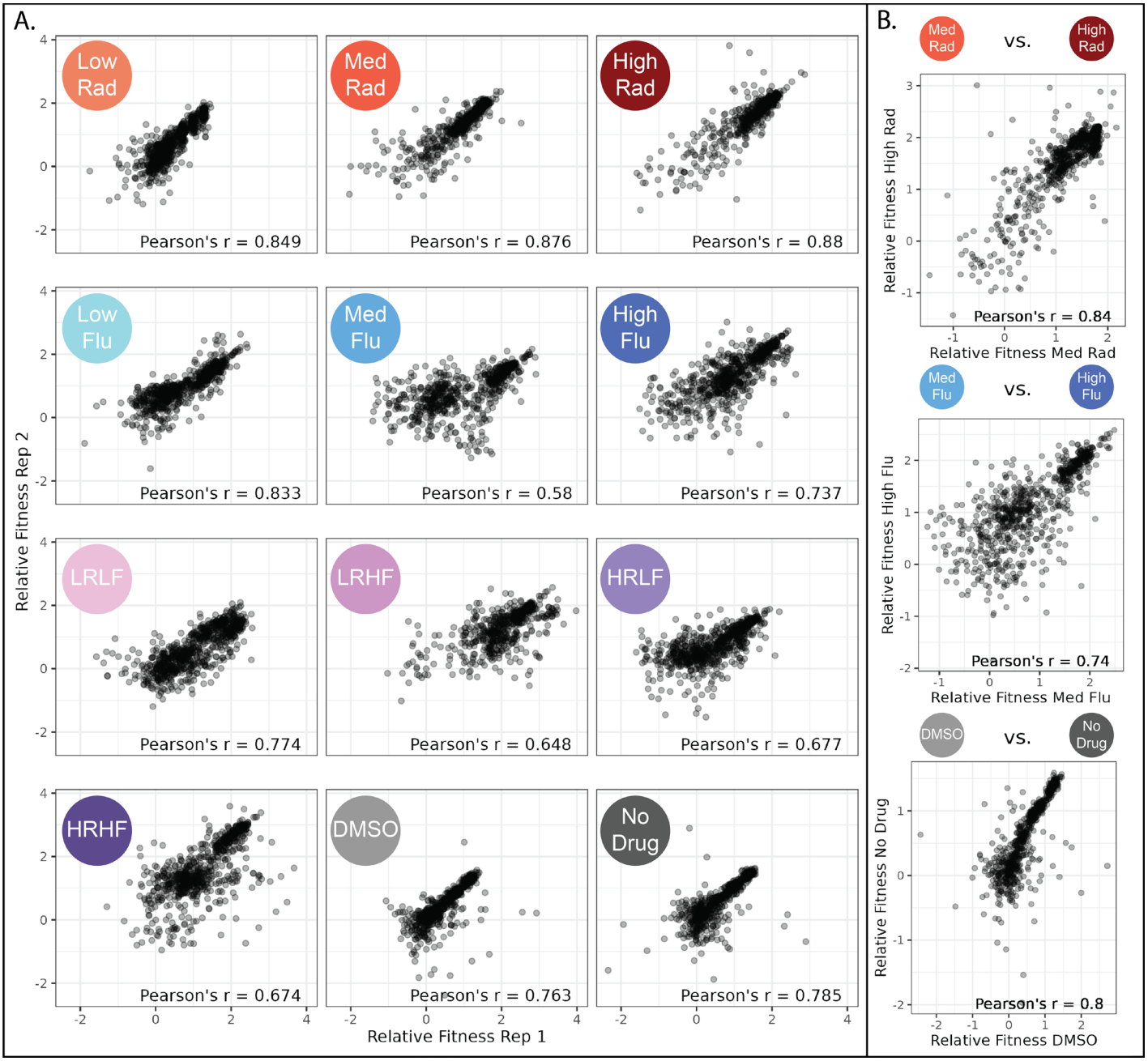

Figure S4: Fitness measurements are reproducible between replicates and closely related conditions.
A. Every point depicts one of the evolved lineages that was observed more than 500 times in both replicates of the fitness competition experiment for a given condition. The average Pearson correlation across all pairs of replicates in all conditions is 0.75. **B.** Every point depicts one of the 774 lineages that was observed more than 500 times in at least one replicate fitness competition. Here, instead of comparing the fitness of replicates, we compare fitness across conditions for 3 closely related pairs of conditions. Comparisons across conditions may be less noisy than those across replicates because fitness in a particular condition represents the average fitness across replicates in that condition.

bioRxiv preprint doi: https://doi.org/10.1101/2023.10.17.562616; this version posted October 20, 2023. The copyright holder for this preprint (which was not certified by peer review) is the author/funder, who has granted bioRxiv a license to display the preprint in perpetuity. It is made available under aCC-BY-ND 4.0 International license.

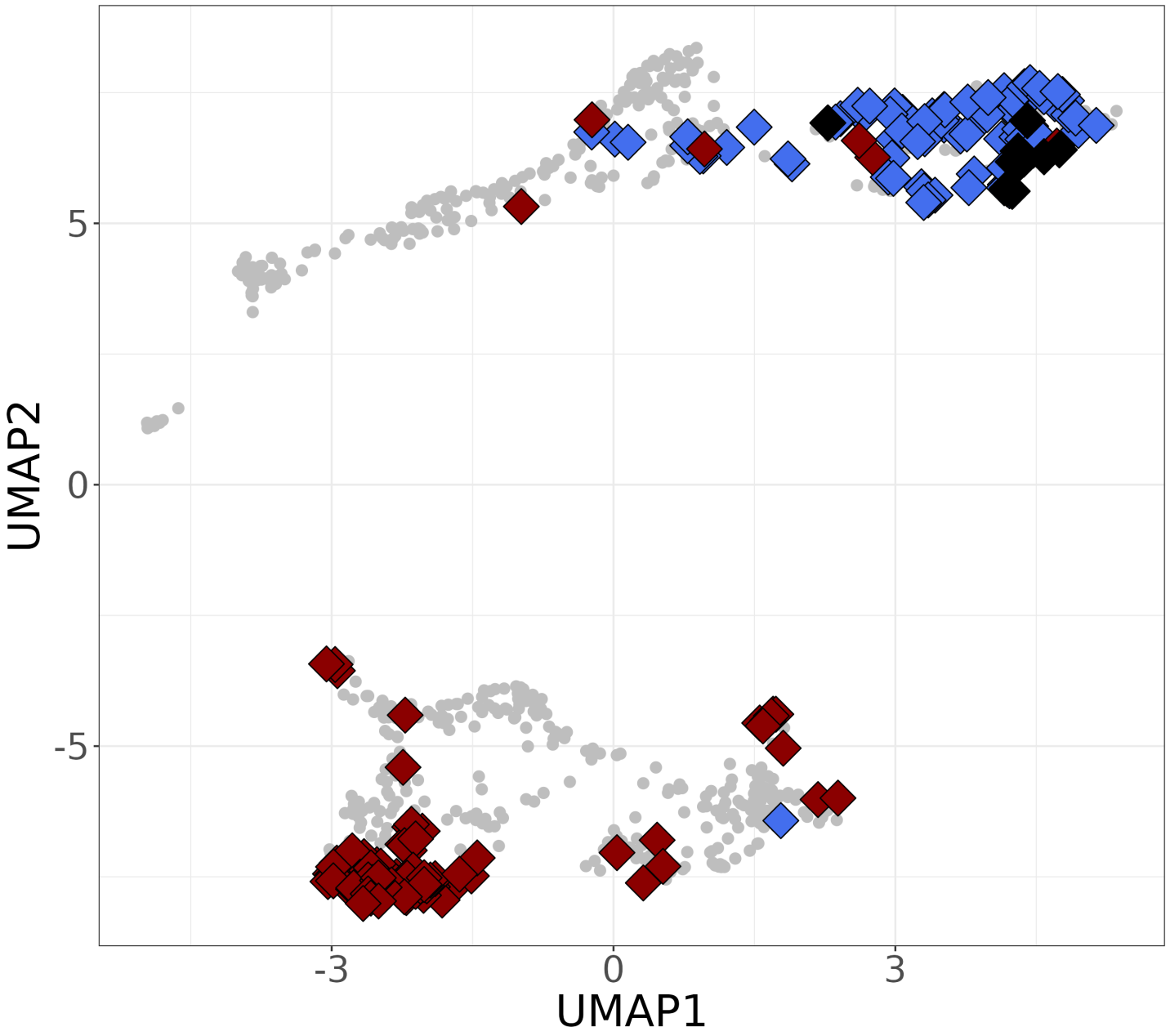

Figure S5: The two types of adaptive mutants depicted in figure 2 sort into different clusters on the UMAP. The top 100 highest fitness lineages in high FLU (blue) and high RAD (red) largely cluster into different groups, with the 7 overlapping mutants (black) falling into the uppermost group.

bioRxiv preprint doi: https://doi.org/10.1101/2023.10.17.562616; this version posted October 20, 2023. The copyright holder for this preprint (which was not certified by peer review) is the author/funder, who has granted bioRxiv a license to display the preprint in perpetuity. It is made available under aCC-BY-ND 4.0 International license.

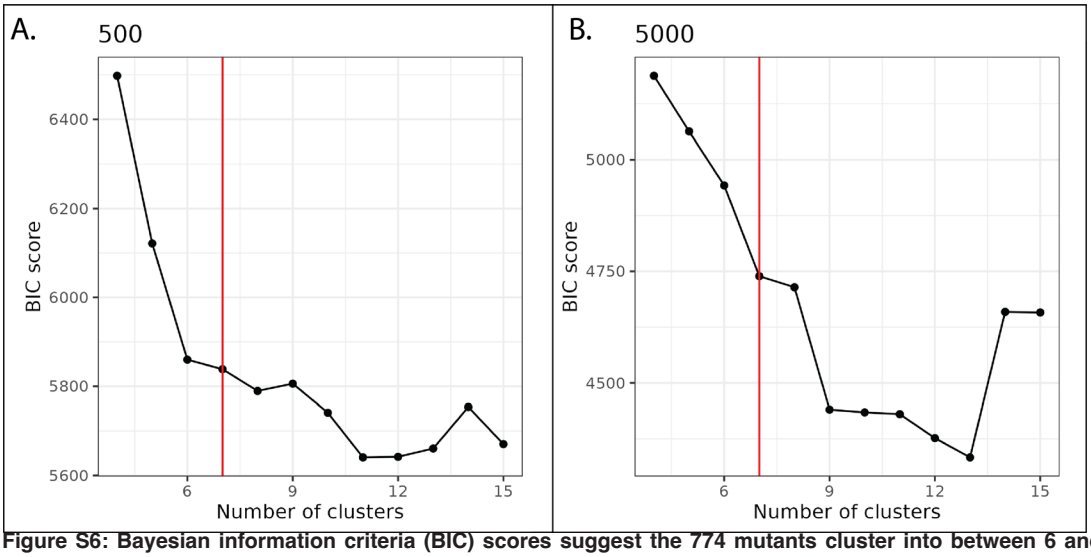

Figure S6: Bayesian information criteria (BIC) scores suggest the 774 mutants cluster into between 6 and 13 groups. We used a gaussian mixture model to distinguish clusters of mutants with unique fitness profiles. A. BIC scores for analysis performed on 774 mutant lineages that each were observed at minimum 500 times per environment. B BIC scores for analysis performed on 617 mutant lineages that each were observed at minimum 5000 times per environment.

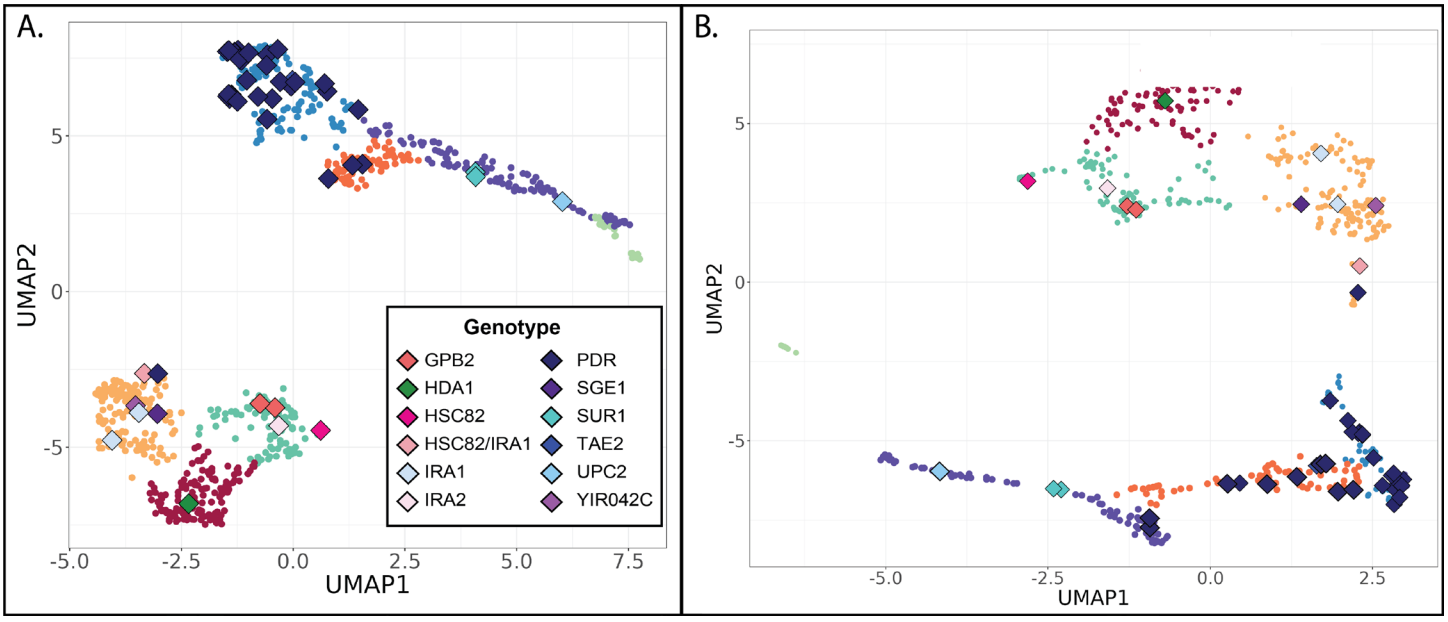

Figure S7. UMAP structure is robust. A. In this UMAP plot, relative fitness of the 774 lineages is fed directly into UMAP prior to normalizing the data to have equal variance across all environments as was done in figure 3D. This has little impact on the appearance of the UMAP. **B.** UMAP made with 617 lineages that were observed more than 5000 times in at least one replicate. While the appearance of the UMAP is inverted relative to figure 3D, the clusters largely retain the same lineages. As lower coverage (noisier) data points are removed from this dataset, the observation that the overall patterns are maintained suggests our original clusters were not based on noisy fitness measurements.

bioRxiv preprint doi: https://doi.org/10.1101/2023.10.17.562616; this version posted October 20, 2023. The copyright holder for this preprint (which was not certified by peer review) is the author/funder, who has granted bioRxiv a license to display the preprint in perpetuity. It is made available under aCC-BY-ND 4.0 International license.

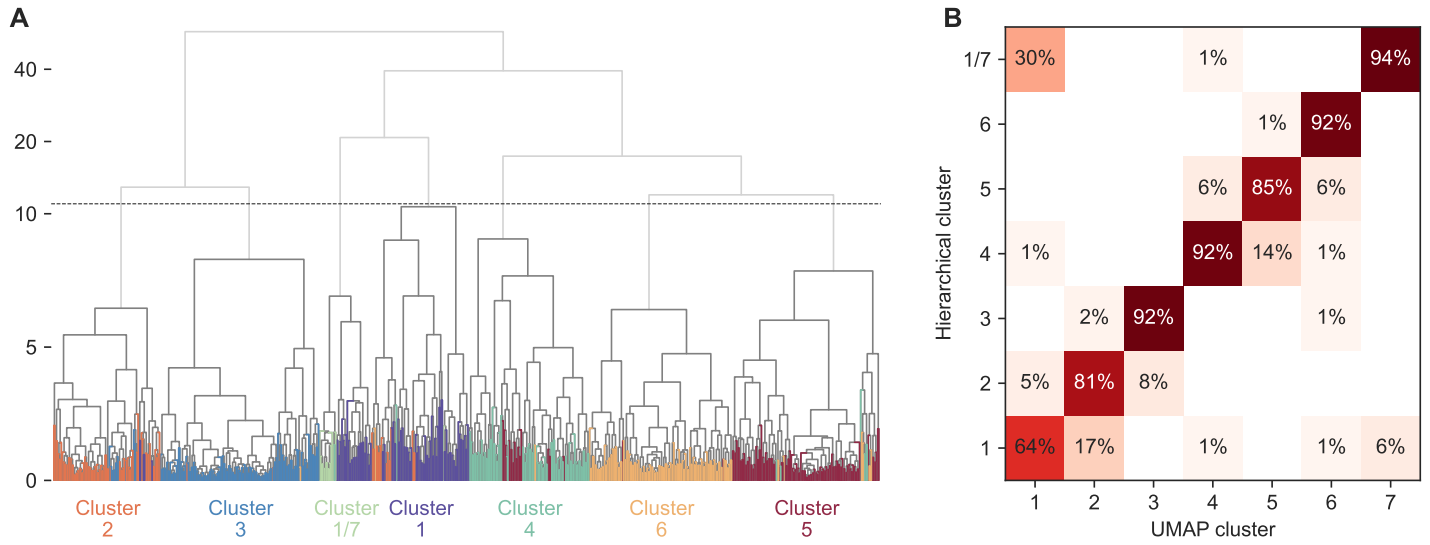

Figure S8. Clusters are robust to a hierarchical clustering method. A. In order to assess whether clusters identified from the UMAP are robust to alternative clustering methods, we used hierarchical clustering to identify clusters of mutants with similar fitness profiles. This figure depicts a dendrogram where the branch length between each lineage (or group of lineages) represents the distance between the clustered groups as measured across all measured conditions. The terminal branch leading to each lineage is colored by that lineage's cluster from the UMAP clustering used in figure 3 of the main text. Dark gray lines show clusters identified using a between-cluster cutoff of 11, which creates 7 clusters, consistent with the number of clusters we identified in figure 3 via clustering on the UMAP space. Hierarchical clusters are labeled and colored corresponding to whichever of the UMAP clusters they share the most overlapping lineages with. Note that the y-axis is linearly scaled between 0 and 10 and log2 scaled above 10 for visualization purposes. **B.** A matrix quantifying how well the results of this hierarchical clustering method correspond with those of the UMAP method presented in figure 3, depicting the percentage of a given UMAP cluster that ends up with each corresponding hierarchical cluster. For the most part, mutants that are clustered together in the UMAP in figure 3 are also clustered together in panel A. Even though it appears that mutants in cluster 1 (which are those most resistant to low FLU) move to a different cluster, these mutants move together to the cluster pertaining to the control strains as they have the least severe effects on fitness.

bioRxiv preprint doi: https://doi.org/10.1101/2023.10.17.562616; this version posted October 20, 2023. The copyright holder for this preprint (which was not certified by peer review) is the author/funder, who has granted bioRxiv a license to display the preprint in perpetuity. It is made available under aCC-BY-ND 4.0 International license.

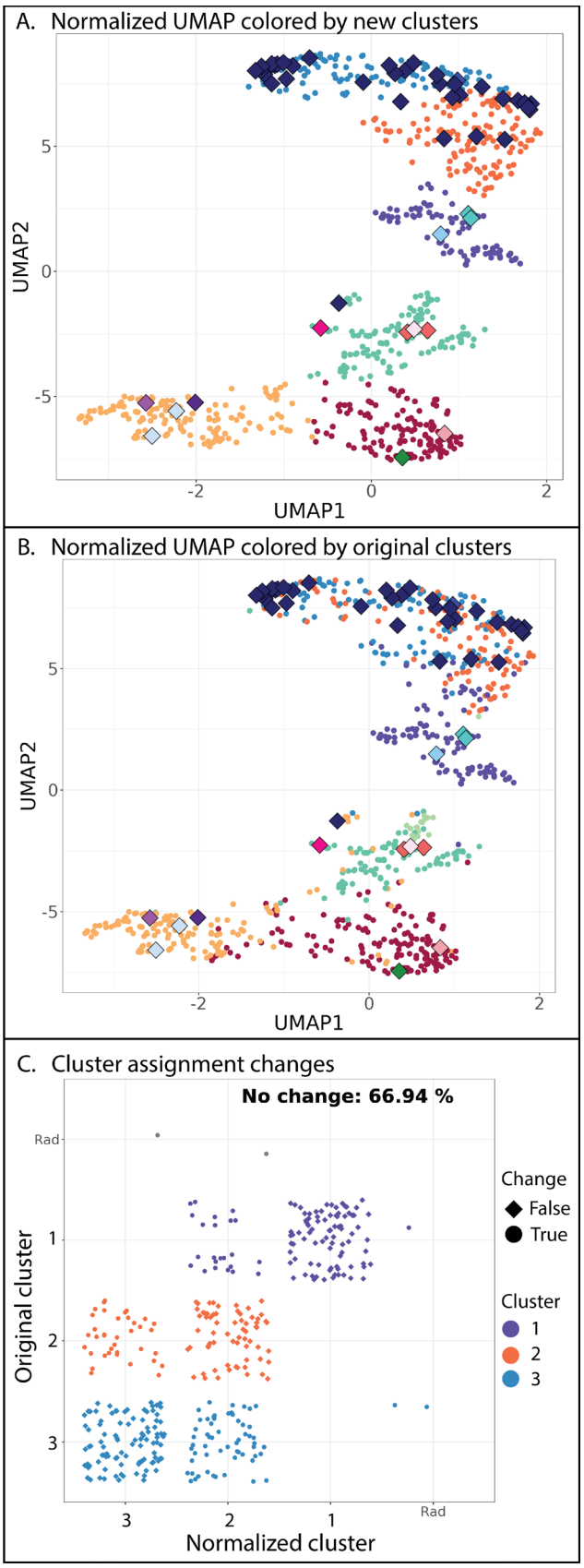

Figure S9: UMAP on data for 774 lineages that were normalized to account for magnitude differences (row means set to 0). A. Every point in this plot represents one of the barcoded lineages colored by cluster; clusters were identified using a gaussian mixture model. The 774 adaptive lineages cluster into 6 groups based on variation in their fitness profiles; the control lineages cluster into the middle cluster in light green. **B.** Original cluster calls were mapped on the new UMAP. While the blue and orange clusters show mixing, other cluster structures are largely retained. C. Plot shows all lineages that are present in cluster 1-3 in either not normalized or normalized dataset. Lineages that do not change clusters are represented by diamonds while those that switch are noted with circles. Nearly 67% of lineages remain in their original cluster after accounting for normalization differences.

bioRxiv preprint doi: https://doi.org/10.1101/2023.10.17.562616; this version posted October 20, 2023. The copyright holder for this preprint (which was not certified by peer review) is the author/funder, who has granted bioRxiv a license to display the preprint in perpetuity. It is made available under aCC-BY-ND 4.0 International license.

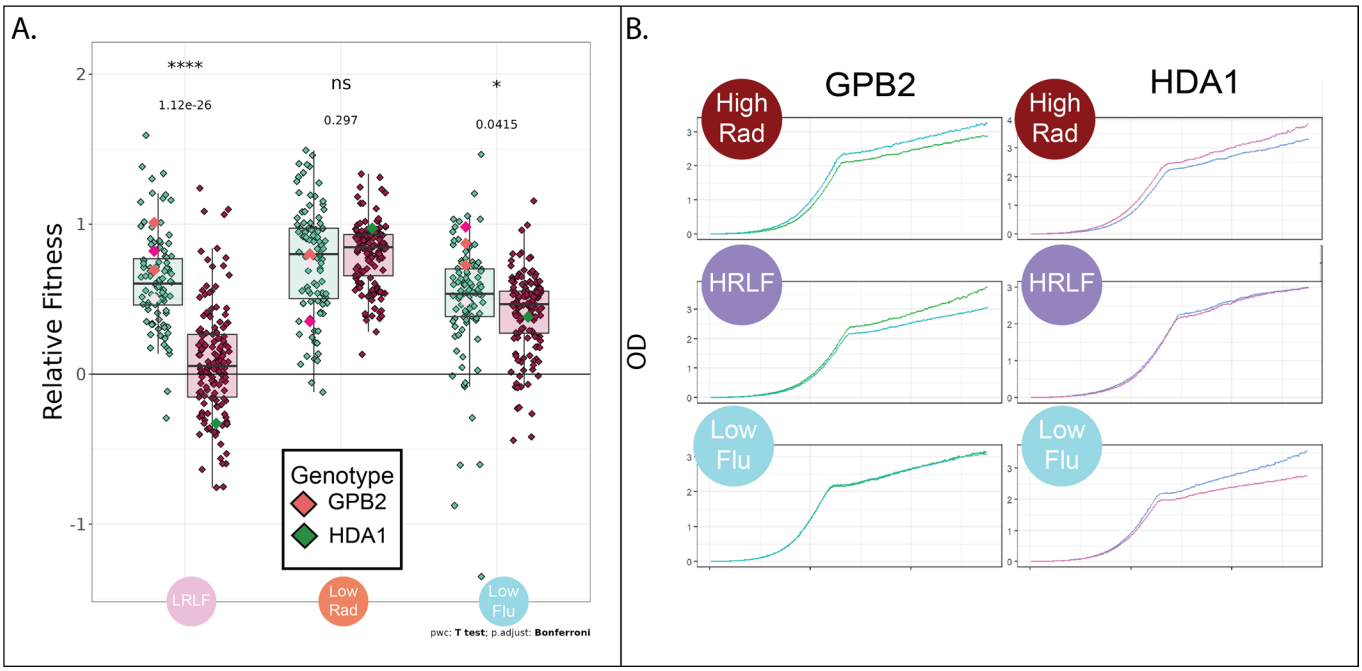

Figure S10: Unexpected tradeoffs in evolved lineages in cluster 4 and 5 in response to combined drugs. A. Cluster 5 (red) has an unexpected fitness disadvantage in the LRLF multidrug environment relative to cluster 4 (green), given that cluster 5 lineages do not have a relative fitness disadvantage in the relevant single drug environments. Boxplots summarize the distribution across all lineages within each cluster in each environment, displaying the median (center line), interquartile range (IQR) (upper and lower hinges), and highest value within 1.5 × IQR (whiskers). **B.** Raw growth curve data for relative maximum growth rates presented in Figure 6D. Two mutants, one to GBP2 (cluster 4) and one to HDA1 (cluster 5) were grown individually in the conditions shown.

bioRxiv preprint doi: https://doi.org/10.1101/2023.10.17.562616; this version posted October 20, 2023. The copyright holder for this preprint (which was not certified by peer review) is the author/funder, who has granted bioRxiv a license to display the preprint in perpetuity. It is made available under aCC-BY-ND 4.0 International license.

Table S1: The sequenced mutations present in each of the adaptive lineages on which we performed whole genome sequencing. https://osf.io/pxyv9/files/osfstorage/6516049b3d9bde04078d871f

Table S2: The percent of isolates from each evolution experiment that became diploid by the timepoint we sampled from.

Evolution Conditions	Diploids detected (96 sampled)	Estimated % diploid
Low Rad	8	8.3%
Med Rad	0	0.0%
High Rad	0	0.0%
Low Flu	9	9.4%
Med Flu	0	0.0%
High Flu	1	1.0%
LR + LF	4	4.2%
HR +LF*	1	1.1%
LR + HF	1	1.0%
HR + HF	3	3.1%
DMSO	6	6.3%
No Drug	9	9.4%

Estimated percentage of diploid cells in each evolution condition, determined using nuclear staining and flow cytometry as described in Materials and Methods. *For the High Radicicol + Low Fluconazole condition, 95 instead of 96 samples were measured due to undetectable growth in one well.